Atmospheric
Chemistry
and Physics

Carbon monoxide distributions from the upper troposphere to the mesosphere inferred from 4.7 µm non-local thermal equilibrium emissions measured by MIPAS on Envisat

B. Funke[1], M. López-Puertas[1], M. García-Comas[1], G. P. Stiller[2], T. von Clarmann[2], M. Höpfner[2], N. Glatthor[2], U. Grabowski[2], S. Kellmann[2], and A. Linden[2]

[1]Instituto de Astrofísica de Andalucía, CSIC, Granada, Spain
[2]Forschungszentrum and University of Karlsruhe, Institut für Meteorologie und Klimaforschung (IMK), Karlsruhe, Germany

Abstract. We present global distributions of carbon monoxide (CO) from the upper troposphere to the mesosphere observed by the Michelson Interferometer for Passive Atmospheric Sounding (MIPAS) on Envisat. Vertically resolved volume mixing ratio profiles have been retrieved from 4.7 µm limb emission spectra under consideration of non-local thermodynamic equilibrium. The precision of individual CO profiles is typically 5–30 ppbv (15–40% for altitudes greater than 40 km and lower than 15 km and 30–90% within 15–40 km). Estimated systematic errors are in the order of 8–15%. Below 60 km, the vertical resolution is 4–7 km. The data set which covers 54 days from September 2003 to March 2004 has been derived with an improved retrieval version including (i) the retrieval of log(vmr), (ii) the consideration of illumination-dependent vibrational population gradients along the instrument's line of sight, and (iii) joint-fitted vmr horizontal gradients in latitudinal and longitudinal directions. A detailed analysis of spatially resolved CO distributions during the 2003/2004 Northern Hemisphere major warming event demonstrate the potential of MIPAS CO observations to obtain new information on transport processes during dynamical active episodes, particularly on those acting in the vertical. From the temporal evolution of zonally averaged CO abundances, we derived extraordinary polar winter descent velocities of 1200 m per day inside the recovered polar vortex in January 2004. Middle stratospheric CO abundances show a well established correlation with the chemical source CH_4, particularly in the tropics. In the upper troposphere, a moderate CO decrease from September 2003 to March 2004 was observed. Upper tropospheric CO

observations provide a detailed picture of long-range transport of polluted air masses and uplift events. MIPAS observations taken on 9–11 September 2003 confirm the trapping of convective outflow of polluted CO-rich air from Southeast Asia into the Asian monsoon anticyclone, which has been described in previous studies. Upper tropospheric CO plumes, observed by MIPAS on this day, were predominantly located in the Northern Hemisphere. Most of these plumes could be related to Southeast Asian pollution by means of backward trajectory calculations. During 20–22 October, southern hemispheric biomass burning was the most likely source of the major CO plumes observed over the Southern Atlantic and Indian Ocean.

1 Introduction

Carbon monoxide (CO) is a key trace species in the lower and middle atmosphere. CO is produced at the surface by incomplete combustion processes related to industry, traffic, or biomass burning. In the troposphere, CO acts as an ozone precursor and is an important contributor to the oxidizing capacity as the main sink of the hydroxyl radical. Due to its tropospheric lifetime of about 2 months, CO is the most frequently used tracer to infer the transport of polluted air masses. Besides methane oxidation, its main atmospheric source is located in the mesosphere and thermosphere by photolysis of CO_2, leading to a pronounced volume mixing ratio (vmr) increase with altitude in the middle atmosphere. This abundance gradient coupled with a long chemical lifetime make CO also an excellent tracer for dynamical studies in the middle atmosphere.

Several remote sensing and in situ instruments provide routine measurements of atmospheric CO from the ground, air, and space. Apart from nadir looking sounders as MO-PITT/Terra (Edwards et al., 2004), SCIAMACHY/Envisat (Frankenberg et al., 2005; Buchwitz et al., 2000; Gloudemans et al., 2008), TES/Aura (Rinsland et al., 2006), and the recently launched IASI/Metop (Turquety et al., 2004), which provide tropospheric CO distributions, there are at present only a few limb sounders operating from space which are capable to observe vertically resolved CO abundances in the lower and middle atmosphere. These instruments employ the microwave i.e. SMR on Odin (Dupuy et al., 2004) or MLS on Aura (Filipiak et al., 2005) or infrared $CO(1\rightarrow0)$ and $CO(2\rightarrow0)$ ro-vibrational transitions at 4.7 and 2.4 μm. In contrast to solar occultation techniques used in the past by ATMOS (Gunson et al., 1990) and recently by ACE-FTS (Clerbaux et al., 2005), measurements of CO from atmospheric infrared emissions, though offering the advantage of global, illumination-independent coverage, are sparse. One of the reasons is that the retrieval of CO from its infrared emissions has to account for strong non-local thermodynamic equilibrium (non-LTE) effects, most pronounced at daytime, demanding sophisticated and time-consuming non-LTE retrieval schemes. Such CO non-LTE retrieval schemes have been applied to ISAMS measurements (López-Valverde et al., 1996) and, more recently, to MIPAS observations (Funke et al., 2007a).

Stratospheric CO distributions derived from MIPAS 4.7 μm non-LTE emissions have been analyzed in previous studies dealing with the polar winter descent of odd nitrogen (Funke et al., 2005; López-Puertas et al., 2005; Konopka et al., 2007). Here, we present MIPAS CO data obtained during September 2003 to March 2004 which has been derived with a revised CO retrieval version. This new version V3O_CO_9+10 has substantially improved compared to previous versions. MIPAS observations and the improved CO retrieval scheme are described in Sects. 2 and 3, respectively. The temporal evolution of zonally averaged CO abundances in the lower and middle atmosphere is discussed in Sect. 4. The potential of MIPAS CO observations to obtain new information on transport processes during dynamical active episodes in the middle atmosphere is demonstrated in Sect. 5 by means of a case study of the Northern Hemisphere (NH) major warming event in December 2003/January 2004. In Sect. 6, we analyze upper tropospheric CO distributions observed during the Southern Hemisphere (SH) biomass burning season in September/October 2003 with respect to long-range transport patterns and uplift processes of polluted air masses.

2   MIPAS observations

The Michelson Interferometer for Passive Atmospheric Sounding (MIPAS) is a mid-infrared Fourier transform limb emission spectrometer designed and operated for measurement of atmospheric trace species from space (European Space Agency, 2000; Fischer et al., 2008). It is part of the instrumentation of the Environmental Satellite (ENVISAT) which was launched into its sun-synchronous polar orbit of 98.55° N inclination at about 800 km altitude on 1 March 2002. MIPAS passes the equator in southerly direction at 10:00 a.m. local time 14.3 times a day, observing the atmosphere during day and night with global coverage from pole to pole. The instrument's field of view is 30 km in horizontal and approximately 3 km in vertical direction. MIPAS operated from July 2002 to March 2004 at full spectral resolution of 0.035 cm^{-1} (unapodized) in terms of full width at half maximum. During this period, MIPAS recorded a rear-viewing limb sequence of 17 spectra each 90 s, corresponding to an along track sampling of approximately 500 km and providing about 1000 vertical profiles per day in its standard observation mode. Tangent heights covered the altitude range from 68 down to 6 km with tangent altitudes at 68, 60, 52, 47, and then at 3 km steps from 42 to 6 km. After an instrument failure in March 2004, MIPAS resumed operation in a optimized spectral resolution mode with a variety of scan patterns providing different altitude coverage, horizontal and vertical sampling. The raw signal is processed by the European Space Agency (ESA) to produce calibrated geolocated limb emission spectra, labeled level 1-B data (Nett et al., 1999). For this study, level 1-B version 4.61/62 data (so-called reprocessed data) have been used.

3   CO retrievals

CO abundance profiles are retrieved with the scientific MIPAS level 2 processor developed and operated by the Institute of Meteorology and Climate Research (IMK) in Karlsruhe together with the Instituto de Astrofísica de Andalucía (IAA) in Granada. The general retrieval strategy, which is a constrained multi-parameter non-linear least squares fitting of measured and modeled spectra, is described in detail in von Clarmann et al. (2003a,b). Its extension to retrievals under consideration of non-LTE is described in Funke et al. (2001). For radiative transfer modeling, the Karlsruhe Optimized and Precise Radiative transfer Algorithm (KOPRA) (Stiller et al., 2002) is used. Non-LTE vibrational populations of CO and interfering species are modeled with the Generic RAdiative traNsfer AnD non-LTE population Algorithm (GRANADA) (Funke et al., 2002) within each iteration of the retrieval. A description of the treatment of non-LTE in the CO retrievals is provided in Sect. 3.1.

CO vmrs are retrieved from the 4.7 μm spectral region, covered by the MIPAS band D (1820–2410 cm^{-1}), using ro-vibrational emissions of the $^{12}C^{16}O(1\rightarrow0)$ band. Minor radiance contributions of the $^{12}C^{16}O$ first hot band and isotopic fundamental bands are also considered. The main interfering species in this spectral interval are O_3, CO_2, and H_2O.

Prior to the retrieval of CO abundances, the following quantities are retrieved from individual MIPAS measurements and the resulting profiles are used as a priori information in the CO retrievals: residual spectral shift, temperature and line of sight (von Clarmann et al., 2003b), water vapor, and ozone.

The retrievals are performed from selected spectral regions (micro-windows) which vary with tangent altitudes in order to optimize computation time and minimize systematic errors (Echle et al., 2000). Thus, height-dependent combinations of micro-windows were selected with a trade-off between computation time and total retrieval error.

Spectral contamination by clouds and aerosol particles is an important issue for the CO retrievals in the upper troposphere and lower stratosphere. For this reason, specific care has been taken to exclude all spectra of particle-contaminated scenes from the data analysis. Rejection of cloud/aerosol contaminated MIPAS spectra was performed according to the color ratio method of Spang et al. (2004) who used the ratio of the spectral regions 788.2–796.25 cm^{-1} and 832.3–834.4 cm^{-1}, the so-called cloud index CI, to detect a cloud/aerosol signal in the spectra. We use a CI threshold of 4.0 for rejection of contaminated spectra.

The retrieval is performed on an altitude grid of 1 km step widths up to 50 km, 2–2.5 km steps between 50 and 80 km and 5–10 km steps above. Due to the over-sampled retrieval grid compared to the tangent height spacing, the retrieval is regularized by a Tikhonov-type constraint which adds to the objective function of the least squares fit a penalty keeping the differences of mixing ratios at adjacent altitudes reasonably small (Tikhonov, 1963; Steck, 2002). This is achieved by using a smoothness constraint matrix of the type $\gamma \mathbf{L_1^T L_1}$ where γ is a scaling profile and $\mathbf{L_1}$ is a first order finite differences operator. The use of the latter does not constrain the column information but only how this information is distributed over altitude and, thus, provides a bias-free retrieval. In addition to the target retrieval parameters, a height- and wavenumber-independent radiance offset and a continuum-like optical depth profile are fitted jointly for each micro-window in order to compensate for offset calibration errors and atmospheric contributions of weak wavenumber dependence not reproduced by the radiative transfer forward model (von Clarmann et al., 2003b).

CO retrievals presented here were performed with the retrieval versions V3O_CO_9 and V3O_CO_10 which are significantly improved compared to previous versions. A major improvement represents the inversion of log(vmr) instead of vmr which allows to better account for the pronounced temporal and spatial variability of the CO vmr, particularly in the winter hemisphere, by reducing the dynamical range of the retrieval parameter vector. The use of log(vmr) further implies an inverse scaling of the Jacobian matrix with the CO vmr, resulting in a stronger regularization effect at CO profile regions with low vmrs compared to those with high vmrs. In consequence, one single regularization strength scaling profile γ can be used for all latitudes and seasons without run-ning the risk of retrieving over-regularized or meaningless (i.e. precision $\gg$100%) profiles.

In order to account for the impact of the vmr profile shape above the uppermost tangent height on the retrieved CO vmrs, we apply seasonal and latitude-dependent a priori profiles taken from chemical transport model calculations (Garcia, 1983). The regularization strength scaling profile was chosen iteratively by means of test retrievals such that the impact of the a priori profile on the retrieved CO abundances is negligible below 65 km, while the retrieval precision generally stays below 80%. The latter constraint is required to avoid a possible positive bias in the statistical analysis of CO data retrieved on the basis of log(vmr).

Spectral micro-windows applied to retrieval versions V3O_CO_9 and V3O_CO_10 were selected in the 2040–2120 cm^{-1} range which covers the stronger P-branch of the $^{12}C^{16}O$ fundamental band. This micro-window selection provides a better sensitivity to the upper troposphere and polar winter stratosphere compared to previous retrieval versions. Further improvements of retrieval versions V3O_CO_9 and V3O_CO_10 include innovative methods for consideration of non-LTE populations along the line of sight (LOS) close to the terminator and horizontal vmr gradients in latitudinal and longitudinal directions, which are discussed in detail in Sects. 3.2 and 3.3, respectively.

Differences between retrieval versions V3O_CO_9 and V3O_CO_10 are restricted to minor changes in the non-LTE population calculation setup which is discussed in the next section. Since these changes introduce only small differences in the retrieved CO vmrs which never exceed 5%, we discuss both CO data versions together. The currently available V3O_CO_9+10 data set, used in this study, includes retrieved CO profiles obtained from MIPAS measurements taken in the standard observation mode at full spectral resolution on 54 days between 9 September 2003 and 25 March 2004 (see Table 1). This data set has been cross-validated with ACE-FTS CO observations (Clerbaux et al., 2008). Differences between the ACE-FTS and MIPAS profiles are within ± 26% at all altitudes, except between 38 and 41 km where it reaches 50%. These differences are linked to the very unusual situation of strong CO-downward transport in the Arctic polar vortex in 2004, where most of the coincidences between ACE-FTS and MIPAS are located. The pronounced spatial variability close to the vortex boundary introduces significant differences in the CO distributions at MIPAS and ACE locations even within the coincidence criterion of 18 h in time and 800 km in space. When all the data above 70° N are filtered out, the differences were found to be further reduced.

3.1 Consideration of non-LTE effects

The 4.7 μm spectral region used in the retrieval of CO abundances is affected by non-LTE emissions of CO and O$_3$. Within the retrieval, vibrational populations of these species are calculated with GRANADA for the actual geophysical

Table 1. Daily coverage of the V3O_CO_9+10 data set. Available days (including about 1000 vertical profiles each) are indicated by the last digits of the retrieval version. Unavailable days are denoted by stars.

Month	1	2	3	4	5	6	7	8	9	10	11	12	13	14	15	16	17	18	19	20	21	22	23	24	25	26	27	28	29	30	31
Sep 2003	*	*	*	*	*	*	*	*	10	10	10	*	*	*	10	10	10	*	*	*	*	*	10	10	10	*	*	*	*	*	
Oct 2003	*	*	*	*	*	*	*	*	*	*	*	*	10	10	10	*	*	*	*	10	10	10	*	*	*	9	*	*	9	10	10
Nov 2003	9	9	10	10	9	*	*	10	10	10	9	*	*	*	10	10	10	9	*	10	9	10	*	*	*	*	9	10	10	10	
Dec 2003	*	*	*	*	*	*	*	*	9	*	*	*	*	*	*	*	9	*	*	*	*	*	*	9	*	*	*	*	*	*	*
Jan 2004	9	*	*	*	*	*	*	9	*	*	*	*	*	*	*	9	*	*	*	*	*	*	*	9	*	*	*	*	*	9	*
Feb 2004	*	*	*	*	*	*	*	*	9	*	*	*	*	*	*	*	*	*	*	*	*	9	*	*	*	*	*	9	*		
Mar 2004	*	*	*	9	*	*	*	*	*	*	*	9	*	*	*	*	9	*	*	*	*	*	9	*	*	*	*	*	*	*	*

conditions. This generic non-LTE algorithm provides vibrational and rotational non-LTE populations for relevant atmospheric IR emitters by solving iteratively statistical equilibrium (SEE) and radiative transport equations (RTE) under consideration of radiative, collisional and chemical excitation processes. A detailed description of the 4.7 μm non-LTE modeling is given by Funke et al. (2007a). Here, we summarize briefly the most important non-LTE processes affecting the measured limb radiances and the assessed accuracy of the non-LTE modeling.

Non-LTE vibrational populations of CO are affected by radiative processes (spontaneous emission, absorption of solar radiation, and exchange of photons with the atmosphere and with the surface) and collisions with O_2, N_2, and O. During daytime, CO vibrational populations are largely controlled by absorption of solar radiation at 4.7 and 2.4 μm, leading to an important enhancement of 4.7 μm CO emissions of more than an order of magnitude compared to LTE conditions. At nighttime, the absorption of tropospheric upwelling radiation affects the CO non-LTE populations, however, to a lesser extent than solar excitation during day. Nevertheless, non-LTE effects (i.e., the non-LTE minus LTE difference) in nighttime 4.7 μm limb emissions can be as high as 20% even at altitudes below 40 km. The collisional coupling of CO with $N_2(v=1)$ and $CO_2(v_3)$ via vibration-vibration (V-V) energy transfer represents an important excitation mechanism for $CO(v=1)$ during day and raises the necessity to perform the non-LTE modeling of CO_2 and N_2 prior to the calculation of the CO populations.

Several vibrationally excited O_3 states emit in the 4.7 μm region involving the deactivation of two v_1 or v_3 quanta. The 4.7 μm ozone hot bands show pronounced non-LTE enhancements during daytime due to chemical excitation by $O+O_2+M$. These non-LTE emissions interfere with the CO radiances and thus have to be modeled, too.

The CO non-LTE modeling is performed for the $^{12}C^{16}O(v \leq 2)$ and $^{13}C^{16}O(v=1)$ vibrational levels using lambda iteration and line-by-line radiative transfer. In contrast to retrieval version V3O_CO_9, where a constant average solar flux was assumed in the radiative transfer calculations, version V3O_CO_10 includes a time-dependent solar flux which takes into account the orbital variations of the Sun-Earth distance. This improvement avoids errors of

the CO vibrational populations of 3% at maximum, depending on the season. The CO_2 and N_2 vibrational populations are modeled using the Curtis matrix method including the collisional processes reported by López-Puertas and Taylor (2001) with updates for CO_2 (López-Puertas et al., 2005). For O_3, the steady state equation is solved using a revised collisional scheme and nascent distribution (Kaufmann et al., 2006).

The accuracy of the CO non-LTE modeling has been assessed to be within 5% for the $^{12}C^{16}O$ fundamental band and within 10% for the hot and isotopic bands. We estimate the accuracy of the non-LTE modeling of ozone hot bands included in the spectral micro-windows to be around 5–15% below 45 km, where ozone emissions are strong enough to affect the CO retrieval.

3.2 Correction of LOS non-LTE population gradients

Close to the terminator, vibrational populations of $CO(v=1)$ vary considerably along the line of sight (LOS). Solar excitation leads to increased populations at the illuminated part of the LOS compared to the dark part by as much as one order of magnitude. This is illustrated in Fig. 1 for a particular scan taken at 70.5° N/157° W on 30 January 2004 with a solar zenith angle (SZA) of 90.2° at the center of scan. Here, $CO(v=1)$ population profiles have been calculated with GRANADA at SZAs between 80° and 100° for the geophysical conditions of this location. These LOS population gradients can lead to significant errors in the retrieved CO vmrs if horizontal homogeneity of the vibrational populations is assumed in the forward radiance calculation. Apart of systematic errors, these LOS population gradients can also cause severe convergence problems in the retrieval, particularly under polar winter conditions. In previous CO retrieval versions assuming horizontal homogeneity in the forward calculation, we found that only 5% of the retrievals of polar winter scans close to the terminator have converged, compared to the average convergence of 97% at other conditions.

Therefore, we have included an explicit calculation of the population gradients for center-of-scan SZAs between 70 and 100° in retrieval versions V3O_CO_9+10 in the following manner: CO non-LTE populations are calculated for various SZA within ± 10° around the center-of-scan SZA in the first iteration of the retrieval. The ratios of these populations
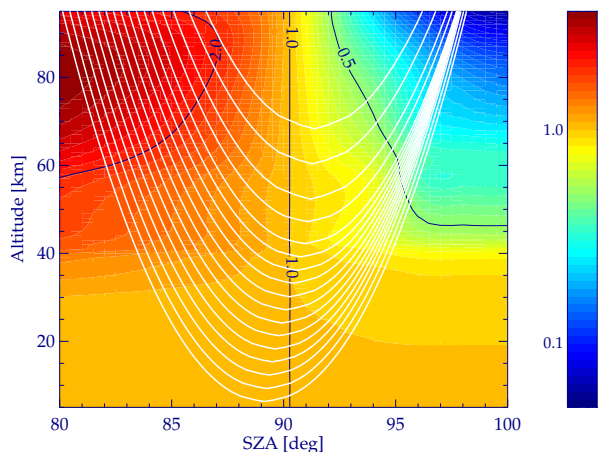
Fig. 1. Modeled illumination-induced variations of CO(v=1) vibrational populations versus solar zenith angle (SZA) along the line of sight for a MIPAS scan taken on 30 January 2004 at 20:51:07 UT centered at 70.5° N/157° W. Population variations are relative to the SZA at the center of scan. Optical pathes of the measured sweeps are indicated as white lines, whereby the satellite position is left of the center of scan.

Fig. 2. Modeled radiances at the line center positions of a strong (P7 at 2115.625 cm^{-1}, red) and weak (P23 at 2046.275 cm^{-1}, blue) CO fundamental band transition versus tangent height with (solid) and without (dotted) consideration of illumination-induced gradients of CO(v=1) populations along the line of sight for the same MIPAS scan as in Fig. 1. Measured tangent heights are indicated by squares.

and the center-of-scan-populations are then used in the following forward calculations to correct the non-LTE populations at any LOS locations by interpolating them to the corresponding SZA and multiplying them to the updated center-of-scan populations. As a result, the fraction of converged V3O_CO_9+10 retrievals from polar winter scans close to the terminator is similar to that typically found for average conditions.

Figure 2 shows the difference between simulated radiances for the same scan as shown in Fig. 1 with and without inclusion of LOS population gradients close to the line centers of the weak and strong CO(1→0) P23 and P7 lines, respectively. While the effect of illumination-induced population gradients is moderate at the P23 line center (i.e., < 15%), radiances at the strong P7 line center are underestimated up to 40% without consideration of population gradients. The effect of population gradients is more pronounced in the stronger P7 line due to spectral saturation which reduces the radiance contribution of the tangent layer compared to layers which contribute farther away from the center of scan. Since in this particular case, CO(v=1) populations increase along the LOS towards the instrument, radiances are increased compared to the simulation considering horizontal homogeneity. Weaker spectral lines as P23 are less saturated and the major radiance contribution originates at the tangent layer close to the center of scan. Therefore, weak spectral lines are less affected by LOS population gradients. The different response of weak and strong lines to these gradients is responsible for the convergence problems encountered in CO retrievals close to the terminator when assuming horizontal homogeneity which disables a simultaneous adjustment of
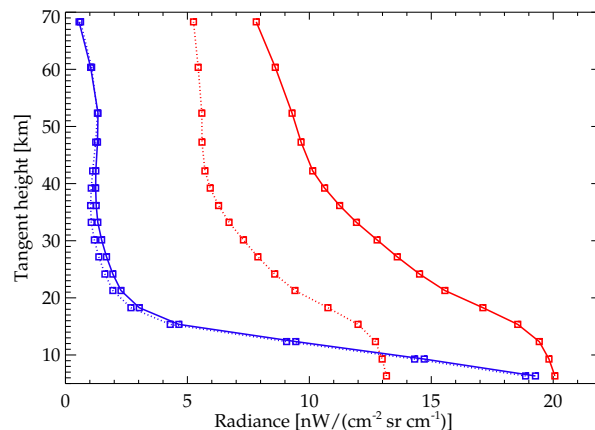
CO lines of different line strengths. Enhanced mesospheric and upper stratospheric CO abundances during polar winter lead to stronger spectral saturation and hence, to higher occurrence of non-convergence in the CO retrievals which assume horizontal homogeneity of CO vibrational populations.

It should be noted that the effect of non-LTE population gradients, as discussed above for a particular scan taken at 70.5° N, is representative for MIPAS terminator overpasses in the NH. The MIPAS viewing direction at the SH terminator is opposite with respect to the day/night-side such that the neglect of non-LTE population gradients generally introduce an overestimation of simulated CO radiances, there.

3.3 Simultaneous retrieval of horizontal vmr gradients

Middle atmospheric CO distributions are characterized by a pronounced spatial inhomogeneity, particularly close to the polar vortex boundary. Horizontal vmr gradients along the LOS affect the retrieval of CO abundances in a similar way as LOS non-LTE population gradients close to the terminator. However, in contrast to the latter, vmr gradients cannot be modeled a priori. In the retrieval version V3O_CO_9+10 we thus retrieve, jointly with the CO vmr, horizontal vmr gradient profiles in latitudinal and longitudinal directions from a single MIPAS scan. These zonal and meridional gradients are defined as a relative vmr change per kilometer in easterly and southerly directions, respectively, at the center of scan location and a given altitude. CO abundances along the LOS are corrected accordingly to these gradients during the ray-tracing procedure performed within the forward calculation of each retrieval iteration.
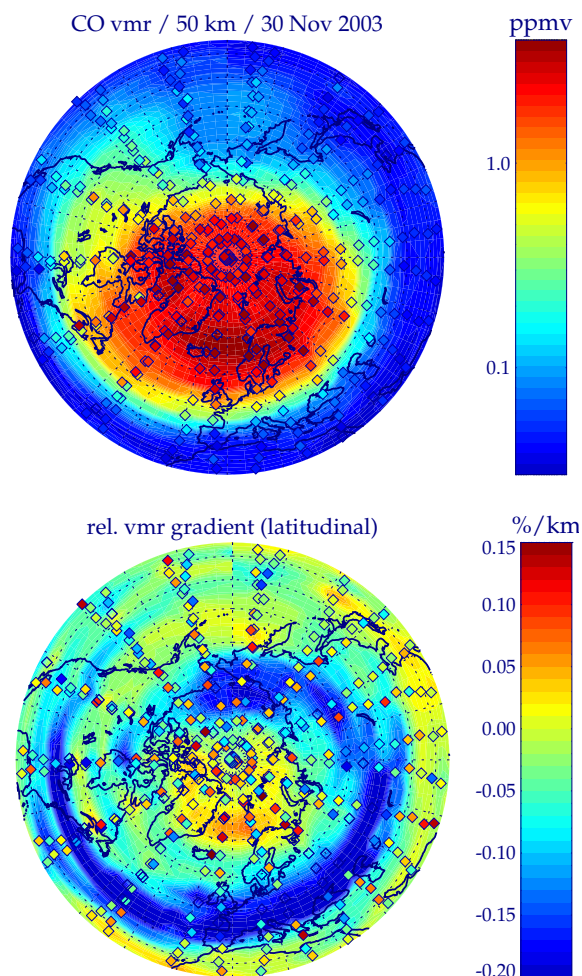
CO vmr / 50 km / 30 Nov 2003

rel. vmr gradient (latitudinal)

Fig. 3. Top: Retrieved CO vmrs from individual observations at 50 km (colored diamonds) observed in the NH on 30 November 2003. The underlaid contours are constructed from the observations by distance-weighted averaging of all measurements within $\pm 10°$ latitude/$\pm 20°$ longitude around each grid point. Note the logarithmic color scale. Bottom: Jointly retrieved meridional vmr gradients from individual observations (colored diamonds). The underlaid contour represents the NUMERICAL gradients obtained from the smoothed CO field shown in the upper panel.

As already discussed in Sect. 3.2, horizontal gradients have a significant impact on the observed spectra only in the case of spectral saturation (i.e., broad radiance contribution functions). If radiative transfer along the LOS is rather linear, no independent information on the horizontal gradients can be gained. In order to avoid an under-constrained retrieval in the case of weakly or unsaturated spectra, we include an optimal estimation regularization for the vmr gradients which forces them to a zero a priori profile if insufficient spectral information is available. The elements of the diagonal covariance matrix used as regularization operator have been chosen such that the retrieved gradients are generally less than 0.3% per km.

Due to the fact that spatial CO distributions may show rather complex structures even within the limited region sounded by a particular MIPAS scan, the applied procedure represents a first-order correction which in particular cases might not be fully able to resolve the "true" spatial CO distribution along the LOS, particularly in the presence of filaments or other small-scale structures. For our application, however, this is of minor importance, since retrieved vmr gradients are only fitted in order to improve the CO vmr retrieval and are not further used as a scientific product.

Due to the 98.55° N inclination of the MIPAS orbit, CO retrievals are more strongly affected by meridional vmr gradients. Except for the polar regions, where the azimuthal viewing direction of MIPAS is slightly sidewards, the impact of zonal vmr gradients is small and the retrieved zonal gradient profiles are thus close to zero.

In general, the retrieved vmr gradients are consistent with the spatial CO vmr distribution inferred from MIPAS observations taken during one day. This is demonstrated in Fig. 3, which shows the inferred CO vmr distribution and the corresponding meridional vmr gradients at 50 km on 30 November 2003 in the NH. The CO distribution on this particular day was characterized by a strong and slightly pole-displaced vortex. The lower panel in Fig. 3 includes the meridional vmr gradients obtained numerically from the inferred CO field shown in the upper panel, as well as those retrieved simultaneously with the CO vmr. Numerical and retrieved gradients agree reasonably well in both, location and magnitude. More pronounced differences, particularly at the vortex edge around 70° N/180° E, are produced by a rapid eastward movement of the vortex, leading to a changed vortex boundary location and hence, different gradients retrieved from MIPAS orbits lying close-by and taken at the beginning and end of the day. From the general consistency of the retrieved horizontal vmr gradients with the observed spatial CO distribution we conclude that the described procedure for correcting horizontal vmr inhomogeneities works correctly and hence, allows for improved MIPAS V3O_CO_9+10 data products.

3.4 Error estimation and retrieval characterization

Error estimation is based on linear theory as suggested by Rodgers (2000). The error budget, which has been assessed for a representative data subset including around 3000 CO retrievals from observations taken on 28–30 November 2003, includes the mapping of the measurement noise on the retrieved volume mixing ratios as well as the propagation of uncertainties of model parameters onto the result. In order to account for the different response of the retrieval to different geophysical conditions, we have performed the error analysis separately for typical atmospheric situations, namely polar winter and summer, mid-latitude, and tropical conditions. Figure 4 shows typical CO vmr profiles (obtained from the averages of the retrieved profiles within the corresponding latitude band) and their single measurement precision

Table 2. Total single measurement CO retrieval error for polar winter and summer, mid-latitude, and tropical conditions.

Altitude	Polar winter		Polar summer		Mid-latitude		Tropics	
km	ppmv	%	ppmv	%	ppmv	%	ppmv	%
70	3.0	29	0.020	19	0.37	24	0.22	22
60	1.3	26	0.012	23	0.093	30	0.033	36
50	0.41	21	0.005	18	0.024	25	0.009	30
40	0.13	55	0.007	31	0.012	38	0.011	35
30	0.025	82	0.007	40	0.012	50	0.012	47
20	0.012	75	0.007	35	0.015	75	0.022	80
15	0.010	52	0.006	34	0.018	39	0.026	38
10	0.017	28	0.009	24	0.014	20	0.014	17

for these atmospheric situations. The average precision of the CO single profile retrievals is dominated by the noise-induced retrieval error. Other random error components, mainly temperature and ozone uncertainties related to the limited precision of the respective preceding retrievals, represent only a minor contribution. Below 50 km, the CO retrieval precision is around 5–30 ppbv, which makes about 15–40% for altitudes greater than 40 km and lower than 15 km for any atmospheric condition whilst it reaches 40–90% within 15–40 km except in polar summer for which the precision is 30–35%. At higher altitudes, the relative precision is around 20–30%. It should be noted that the precision of polar winter retrievals depends strongly on the altitude to which upper atmospheric CO has already descended. CO observations within descended air masses have generally a precision of 20–25%.

Non-negligible systematic error sources are uncertainties in the CO and O_3 non-LTE modeling, spectroscopic data, instrumental line shape modeling, and potential biases in the retrieved profiles of temperature and ozone. Apart of the mapping of non-LTE model errors into the retrieved CO profiles, their individual relative contributions are well below 5%. The total systematic CO retrieval error is estimated to be below 10%, except for altitudes around 40 km, where systematic errors increase to about 15%. There, errors are dominated by O_3 non-LTE model uncertainties leading to systematic residuals in the spectral fit which are generally below the instrumental noise (see Fig. 1 of Funke et al. (2007a)). Although the systematic retrieval errors are well below the precision and hence, represent a minor contribution to the total single measurement retrieval error, they cannot be reduced by means of a statistical analysis and represent thus a potential bias. The altitude-dependent total retrieval errors of single CO measurements at different atmospheric conditions are summarized in Table 2.

The application of a multi-parameter non-linear least squares inversion algorithm implies a redistribution of the altitude-dependent spectral information over the CO retrieval grid which is described by the averaging kernel (AK) ma-
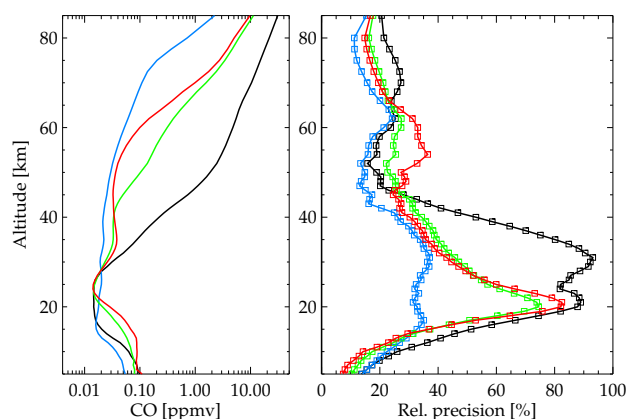

Fig. 4. Retrieved average CO vmr profiles (left) and their relative precision (right) from measurements taken on 28–30 November 2003 for polar winter (black), polar summer (blue), mid-latitudes (green) and tropics (red). The vertical retrieval grid is indicated by squares on the right panel.

trix (Rodgers, 2000). The AK diagonal elements represent a measure of the sensitivity of the CO retrieval at a given profile grid point to the "true" CO vmr. Values close to zero (typically <0.05) indicate that there is no significant sensitivity to the CO abundance at the corresponding altitude. On average, the AK diagonal elements of the V3O_CO_9+10 data are greater than 0.05 in an altitude range of 5–80 km during night and 5–100 km during day. These differences are related to the diurnal variations of the non-LTE vibrational populations of CO. As a consequence, retrieved daytime CO profiles are sensitive to the lower thermospheric CO column, although the limb scans cover only tangent heights up to 70 km.

The vertical resolution of the CO retrieval can be expressed as the full width at half maximum of the AK rows. Figure 5 shows average vertical resolutions of the retrieved CO profiles for polar winter and summer, mid-latitude, and tropical conditions. In the troposphere, vertical resolutions range from 3.5 to 6 km, increasing to 7–8 km in the lower
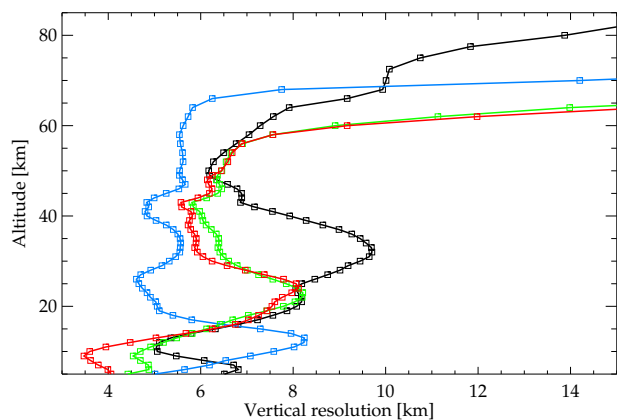
Fig. 5. Average vertical resolution of single measurements, estimated as full width at half maximum of the rows of the averaging kernels, from CO measurements taken on 28–30 November 2003 for polar winter (black), polar summer (blue), mid-latitudes (green) and tropics (red). The vertical retrieval grid is indicated by squares.

stratosphere. In the middle and upper stratosphere, vertical resolutions are around 4.5–6.5 km, except for polar winter conditions where, below the region filled with subsided mesospheric air, vertical resolutions can exceed 8 km. At altitudes above 70 km for polar conditions (60 km in the tropics and mid-latitudes) the vertical resolution increases to values higher than 10 km. Day/night sensitivity differences related to non-LTE cause also differences in the vertical resolution which, however, is only significant at altitudes above 60 km. Therefore, studies of the diurnal variations of mesospheric CO using MIPAS data should include the application of averaging kernels. It should be noted that due to the retrieval of log(vmr), MIPAS CO AKs must always be applied to log(vmr) profiles. The number of independent pieces of information given in the retrieved CO profiles is typically 7.5 (6.5) for day (night) conditions. Polar summer CO profiles can have even up to 9–10 degrees of freedom.

4 Seasonal variations of CO

The V3O_CO_9+10 data set covers approximately half a year (equinox to equinox), thus enabling a study of seasonal variations of CO during 2003/2004 on a global scale. Due to the pronounced spatial variability of CO, particularly in the winter hemisphere, which is mainly generated by planetary wave activity perturbing the polar vortex, seasonal variations of zonal averages are better characterized on equivalent rather than geometrical latitudes. We use potential vorticity from the European Centre for Medium-Range Weather Forecasts (ECMWF) analysis data for the representation of the CO data in equivalent latitudes. Figure 6 shows the temporal evolution of the retrieved CO abundances averaged over equivalent

latitudes 60°–90°, 30°–60°, and 0°–30° during September 2003–March 2004 in both hemispheres.

The temporal evolution of polar CO abundances is characterized by winter descent and summer ascent induced by the meridional circulation leading to high winter and low summer CO mixing ratios. In the SH polar middle atmosphere (Fig. 6, top left), the equinox CO distribution in September 2003 was characterized by descended CO-rich air masses from the preceding winter down to the lower stratosphere with volume mixing ratios ranging from 50 ppbv at 25 km to 4 ppmv at 70 km. In the following months, CO abundances at 30–55 km decreased quickly to values of about 20 ppbv (200 ppbv at 70 km) which are typical for summer solstice conditions. Around 25 km, however, remnant mesospheric air masses with CO abundances of 30–50 ppbv were observed until mid November. A similar behavior has also been reported during the preceding NH polar spring season (Konopka et al., 2007; Engel et al., 2006) and from age of air observations over the spring and summer pole (Stiller et al., 2008). In February 2004, mesospheric CO mixing ratios started to raise again, indicating the turnaround of the meridional circulation close to spring equinox. Upper stratospheric CO abundances, however, decreased to minimum values of less than 10 ppbv in February/March. This CO reduction is caused by increased chemical losses related to high OH abundances in sunlit conditions and a similar reduction of CH_4, the major chemical source of CO at these altitudes. CH_4 abundances (not shown) were retrieved simultaneously with N_2O from MIPAS spectra around 8 μm with an accuracy of 10–20% (Glatthor et al., 2005). The CH_4 decrease is produced by photochemical losses involving photolysis and reactions with OH and $O(^1D)$ during polar summer. CO distributions in the SH polar upper troposphere show volume mixing ratios around 20 ppbv without significant seasonal variations.

The extraordinary NH polar winter 2003/2004 (Manney et al., 2005a) is covered entirely by the CO data set presented here (Fig. 6, top right). From September to the end of October 2003, polar winter descent with vertical velocities of 350–400 m per day, as deduced from the vertical shift of the inferred CO vmr mean profiles, led to increases of CO vmrs from 0.5 to 8 ppmv at 70 km (20 to 200 ppbv at 50 km). The fall equinox stratospheric CO minimum which has been observed in the SH in March 2004, showed also up in the NH during September/October 2003. This minimum, first located around 45 km, descended with the circulation to altitudes around 25 km in December. During November and the first half of December, average descent velocities slowed down to 200–300 m per day between 40 to 70 km. During this period, polar vortex perturbations induced moderate variations in the NH polar CO abundances, particularly in the mesosphere. In mid December, a major warming event led to a CO decrease in the upper stratosphere and mesosphere (USM) by shifting CO-rich vortex air masses to mid-latitudes where they mixed with ambient
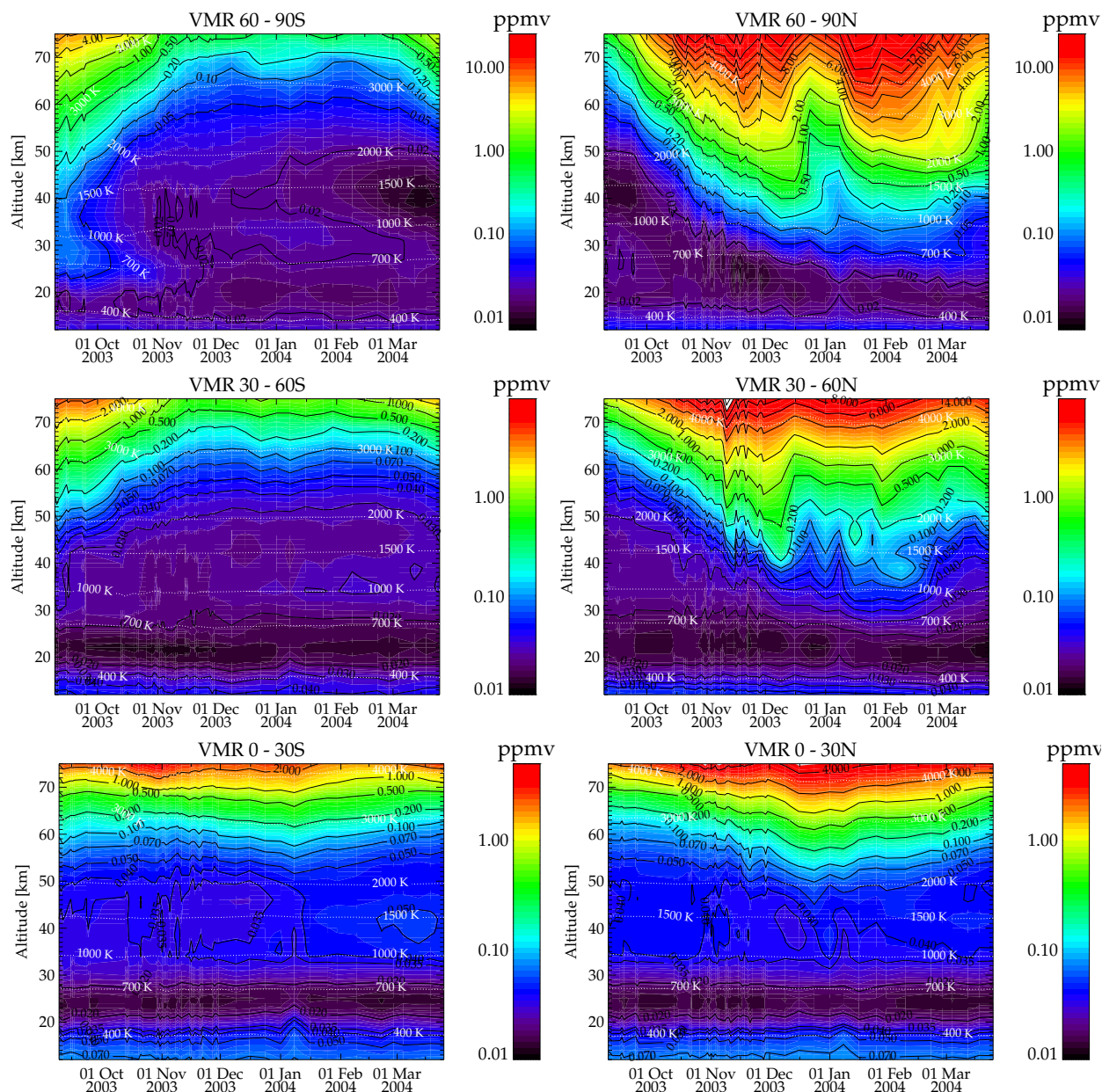
Fig. 6. Temporal evolution of retrieved CO vmrs averaged over equivalent latitudes 60–90° S, 60–90° N, 30°–60° S, 30°–60° N, 0°–30° S, and 0°–30° N (upper left to lower right panels) from September 2003 until March 2004 (note the logarithmic color scale). An area-weighting factor (cosine of equivalent latitude) has been applied. Mean potential temperatures are indicated by dotted white lines. Note that the apparent higher variability during October/November 2003 is related to a finer temporal sampling in this period.

air. The same occurred in the middle stratosphere about 2–3 weeks later. In mid-January 2004, a very strong vortex built up again in the USM, giving raise to an unusually strong descent with velocities of approximately 1200 ± 100 m per day in the mesosphere. Such high descent rates have been reported, to our knowledge, only from model studies (Siskind, 2000). However, extraordinary descent in this period has also been detected from satellite observations of NO_x (Ran-

dall et al., 2005; Rinsland et al., 2005; Hauchecorne et al., 2007; Funke et al., 2007b). End of January, CO vmrs up to 15 ppmv have been observed at 70 km. In February, the strong downward motion decelerated significantly. This is in agreement with results from GOMOS NO_2 observations which show a reduction of descent rates from 600 m/day in the late January to 200 m/day in early March (Hauchecorne et al., 2007). Afterwards, CO abundances began to decrease,
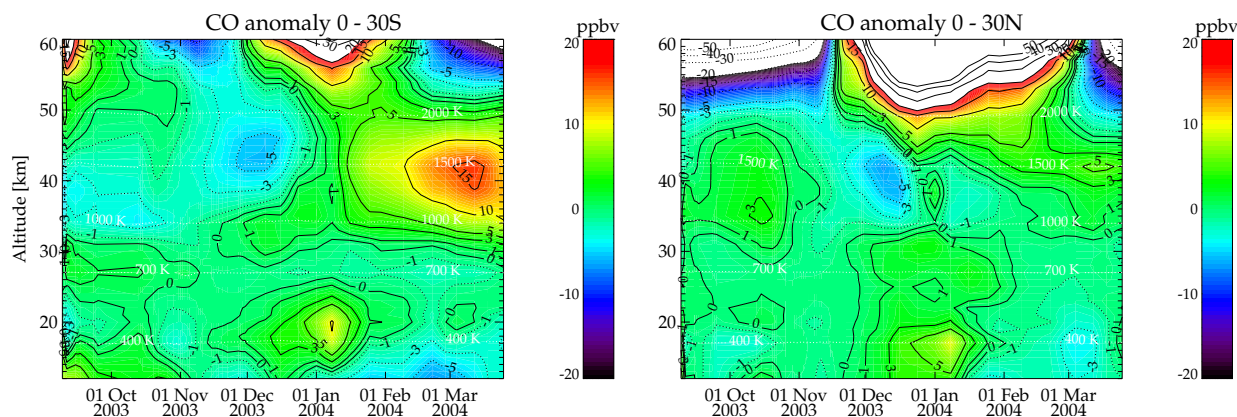
Fig. 7. As Fig. 6 (bottom panels), but shown as CO difference with respect to the mean profile averaged over the full time period. Data is temporally smoothed within 10 days.

more pronounced in the mesosphere than in the stratosphere. Overall, MIPAS CO observations indicate that polar mesospheric air masses descended about 25 km (i.e., from 50 km to 25 km) from November 2003 until March 2004, resulting in an average polar winter descent rate of 5 km/month. This is in good agreement with Nassar et al. (2005) who derived values of 3.2–5.3 km/month in the upper stratosphere and mesosphere from ACE-FTS observations of H_2O, CH_4, and N_2O for the same winter. Rosenfield et al. (1994) also modeled descent in both hemispheres at a range of altitudes and calculated 27 km of descent for air originating at 50 km.

The temporal evolution of the SH mid-latitude CO abundances is very similar to the evolution of polar CO in the summer hemisphere, indicating a well-mixed extra-tropical CO distribution (Fig. 6, middle left). Also in the winter hemisphere (Fig. 6, middle right), similarities with the corresponding polar CO evolution are evident, however, CO abundances are generally lower than at the polar regions, particularly in the second half of the winter after the warming event. The more pronounced CO latitudinal gradient in 2004 is related to the stronger and less extended polar vortex, with its edge located around 70° N equivalent latitude, after its rebuilt in January. In contrast, during the first part of the winter in 2003, the vortex extended generally to 60° N or even lower equivalent latitudes which gave raise for some strong oscillations of the NH mid-latitude CO in the USM during November 2003. During the warming event at the end of December, additional CO was introduced into the NH mid-latitudes which descended during January to altitudes around 35–40 km (showing up as a tongue in the figure) before being mixed with ambient air. Upper tropospheric CO abundances at mid-latitudes show the expected hemispheric differences related to the distribution of tropospheric sources and decreased from about 70 to 40 ppbv (50 to 30 ppbv) during the whole time period in the NH (SH) around 12 km. It is not clear if this decrease is related to the seasonal varia-

tions of the biomass burning activity on a global scale with a maximum around the austral spring equinox or to annual dynamical oscillations.

The tropical CO evolution (Fig. 6, bottom) shows only small variations in the mesosphere which reflect the meridional circulation patterns. Typical vmrs are 1 ppmv at 70 km, decreasing to 50 ppbv at 55 km. In the tropical troposphere and lower stratosphere, typical CO vmrs are around 80–90 ppbv at 12 km, decreasing with altitude to 50 ppbv at 17 km and 20 ppbv at 21 km.

Figure 7 shows the seasonal variations in the tropics as anomaly with respect to the average over the whole period. In the upper troposphere and lower stratosphere, a 5–10 ppbv increase occurred during December and January in both hemispheres. This increase is similar to the tape recorder-like signal linked to the seasonal change of biomass burning, identified by Schoeberl et al. (2006). MLS observations taken during 2005–2006 (Jin et al., 2008) show a similar behavior. A CO decrease from fall to spring equinox is also visible in the tropical upper troposphere, particularly in the SH. However, this decrease of about 10 ppbv is less pronounced than at mid-latitudes. The mid-stratospheric CO abundances show seasonal variations with minimum and maximum abundances of 25 and 55 ppbv, respectively. In the SH, CO vmrs show a pronounced maximum at 40 km around February/March 2004. A second one, however much less pronounced is visible in October 2003. In the NH, the October 2003 and February/March 2004 maxima are similar in terms of magnitude. The mid-stratospheric CO variability is very well correlated to the temporal evolution of the CO precursor, methane, (see Fig. 8, top panel) which has been retrieved from the same MIPAS measurements.

This indicates that, at these altitudes, the CO evolution is mainly driven by chemical processes. CH_4/CO ratios in both hemispheres are very close to a constant value of 20 which is consistent with typical chemical lifetimes of about

3 months and 5 days for CH_4 and CO, respectively, under sunlit conditions around 45 km (Brasseur and Solomon, 1986). The pattern of the mid-stratospheric CO and CH_4 evolution is related to the semi-annual oscillation (SAO) with periods of strongest upwelling during equinox and alternating hemispherical asymmetry. Since the magnitude of the SAO shows pronounced QBO-driven inter-annual variations, we expect a rather high variability of tropical stratospheric CO. A similar tropical CO–CH_4 relation as observed by MIPAS has also been found in long-term model calculations performed with the Whole Atmosphere Community Climate Model (WACCM3), the latter described by Garcia et al. (2007) (see Fig. 8, bottom panel). The average CH_4/CO ratio of 18 in the WACCM3 simulations is very close to the MIPAS observations. However, there is a disagreement with respect to the magnitude of the SAO signal which is smaller in the WACCM3 simulations. Further, the simulations yield a stronger amplitude of the second SAO cycle (maximum during NH fall) in contrast to the MIPAS observations which shows a more pronounced first SAO cycle (maximum during NH spring). This inconsistency of WACCM3 and observed SAOs is known, however, the reason for this still remains to be determined (Rolando Garcia, pers. communication). A further feature showing up in the tropical stratospheric CO evolution observed by MIPAS is a small increase around 37 km at the end of December 2003, being more pronounced in the NH than in the SH. This increase, which is not related to chemical productions by CH_4, is most likely produced by intrusions of mesospheric air masses as consequence of the NH polar stratospheric warming.

5 Stratospheric and mesospheric CO distributions during the NH major warming in December 2003

Due to their dense spatial sampling, MIPAS CO observations provide a comprehensive picture of dynamically active episodes such as stratospheric warmings at upper stratospheric and mesospheric altitudes where traditional tracer like CH_4 or N_2O are not very sensitive. The 2003/2004 NH major warming showed unique characteristics compared to preceding NH winters with mid-winter warmings due to the length of the vortex disruption and the strong and rapid upper stratospheric recovery (Manney et al., 2005a). At the time of its occurrence in December 2003/January 2004, MIPAS was the only remote sensing instrument in space which measured vertically resolved profiles of stratospheric and mesospheric CO. We use V3O_CO_9+10 data to provide a "quasi-synoptic" view of the dynamical situation on several days between 9 December 2003 and 16 January 2004 by means of horizontal and vertical sections through the observed CO vmr distribution.

Since observed CO vmrs show generally a very compact correlation with Ertel's potential vorticity (PV) at fixed potential temperature levels, we use PV from the daily ECMWF
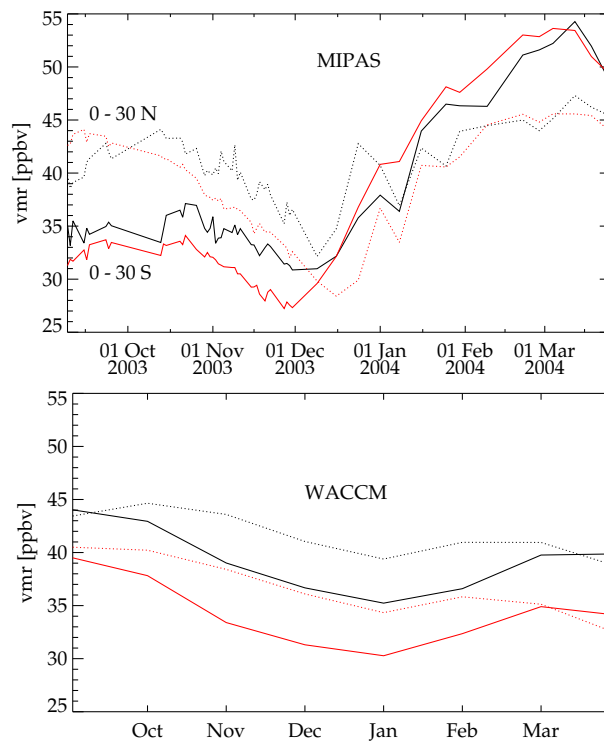

Fig. 8. Top: Temporal evolution of average MIPAS CO (black) and CH_4 (red) abundances at 1500 K potential temperature (approximately 45 km) at equivalent latitudes 0°–30° S (solid) and 0°–30° N (dotted). CH_4 abundances have been scaled by a factor of 0.05. Bottom: As the top panel, but showing the temporal evolution of model CO and CH_4 monthly averages from WACCM3 simulations (Garcia et al., 2007) covering the years 2000–2003.

analysis data to construct CO fields on isentropic surfaces by averaging all observations within ±10° latitude and ±20° longitude around each grid point, weighted by the difference between the PV at the measurement's location/time and the PV at the actual grid point at 12:00 UT. This representation allows for a very detailed view of the CO distribution and how it is driven by dynamical processes. Its validity, however, depends on the quality of the meteorological data used. Thus, we have checked in a first step the spatial consistency of the measured CO data and ECMWF PV contours. The observed CO distributions follow very consistently the isolines of constant PV on all days during the episode (see Figs. 9 and 10). Further, observed spatial CO distributions are very consistent with the CH_4 fields derived from the same MIPAS observations, both species showing a well defined spatial anti-correlation as expected (not shown). Vertical sections through the observed CO distributions are shown as longitudinal cuts at latitudes 80° N and 50° N through the isentropic CO surfaces at potential temperatures between 625 K and 4000 K (Figs. 11 and 12, respectively).
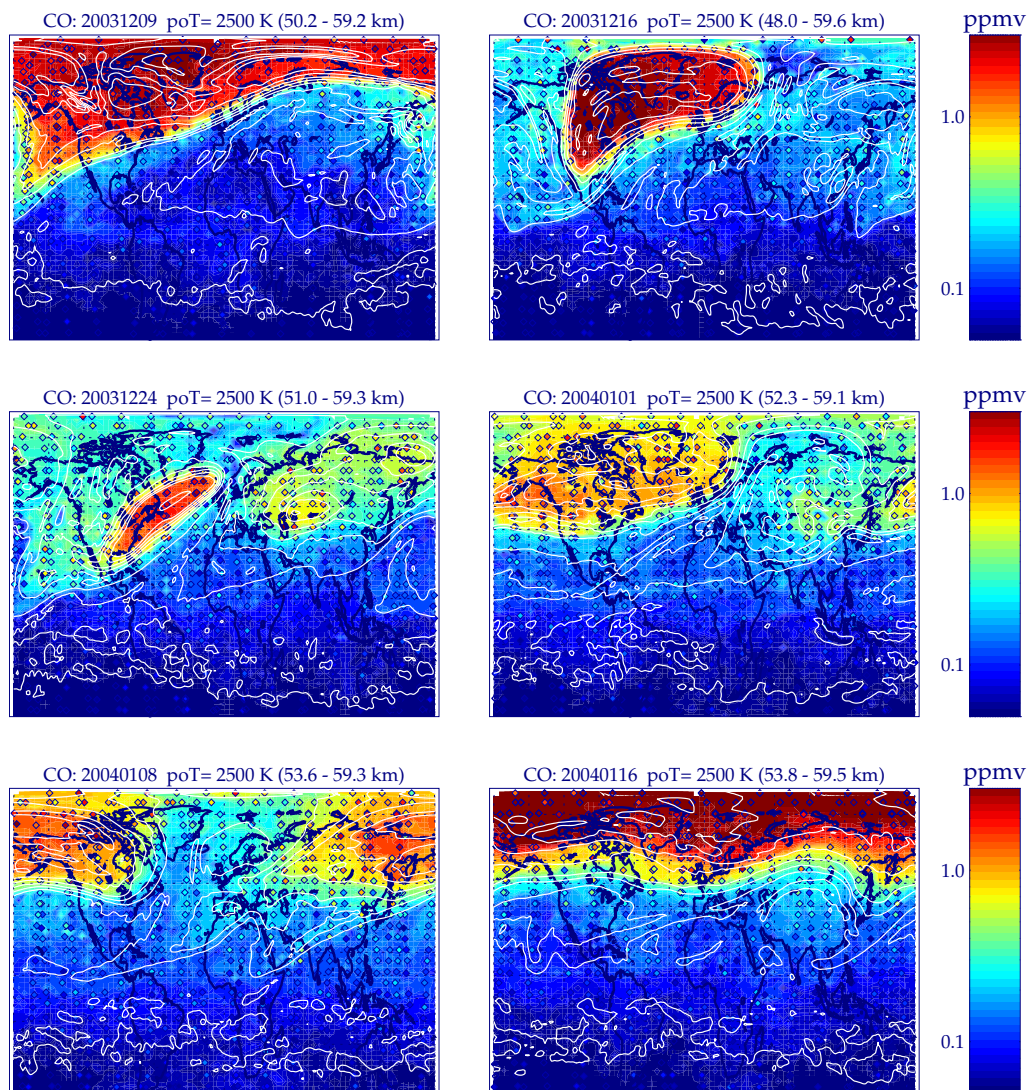
Fig. 9. Observed CO abundances at the 2500 K isentropic surface on several days in December 2003 and January 2004, covering the NH major warming (from top left to bottom right: 9 December, 16 December, 24 December, 1 January, 8 January, and 16 January). Individual MIPAS observations are shown by colored diamonds. The underlaid CO fields are constructed by averaging all measurements within ±10° latitude/±20° longitude around each grid point, weighted by the PV-difference of the measurement's location and the actual grid point. Note the logarithmic color scale. Representative PV contours are shown as white lines.

The 2003/2004 NH warming event was preceded by a strong wave 1 amplification, resulting in an elongated polar vortex in the 30–150° W sector with an extension to latitudes around 30° N on 9 December 2003 (see Figs. 9–12, upper left panels). Mixing of vortex and mid-latitude air occurred westwards of the vortex tail located over the American continent, leading to a region of intermediate CO abundances of 100–200 ppbv at 1500 K. The vortex core, however, was still pole-centered on this day. CO abundances reached 5 ppmv at 3500 K and 0.5 ppmv at 1500 K. Mesospheric air masses were observed down to approximately 1000 K.

On 16 December, the vortex was even stronger shifted towards North America and mid-latitude air poor in CO filled already the North Pole region at 2500 K (see Figs. 9–12, upper right panels). In contrast to the CO decrease at polar latitudes, CO abundances increased significantly inside the shifted polar vortex at 50° N below 2500 K, indicating accelerated descent. At 1500 K, we observe a CO-rich filament expanding from the vortex tail west of California towards China's East coast.

On 24 December, the vortex had moved entirely to latitudes below 80° N at altitudes above 1500 K (see Figs. 9–12, middle left panels). CO abundances of 0.5 ppmv were found
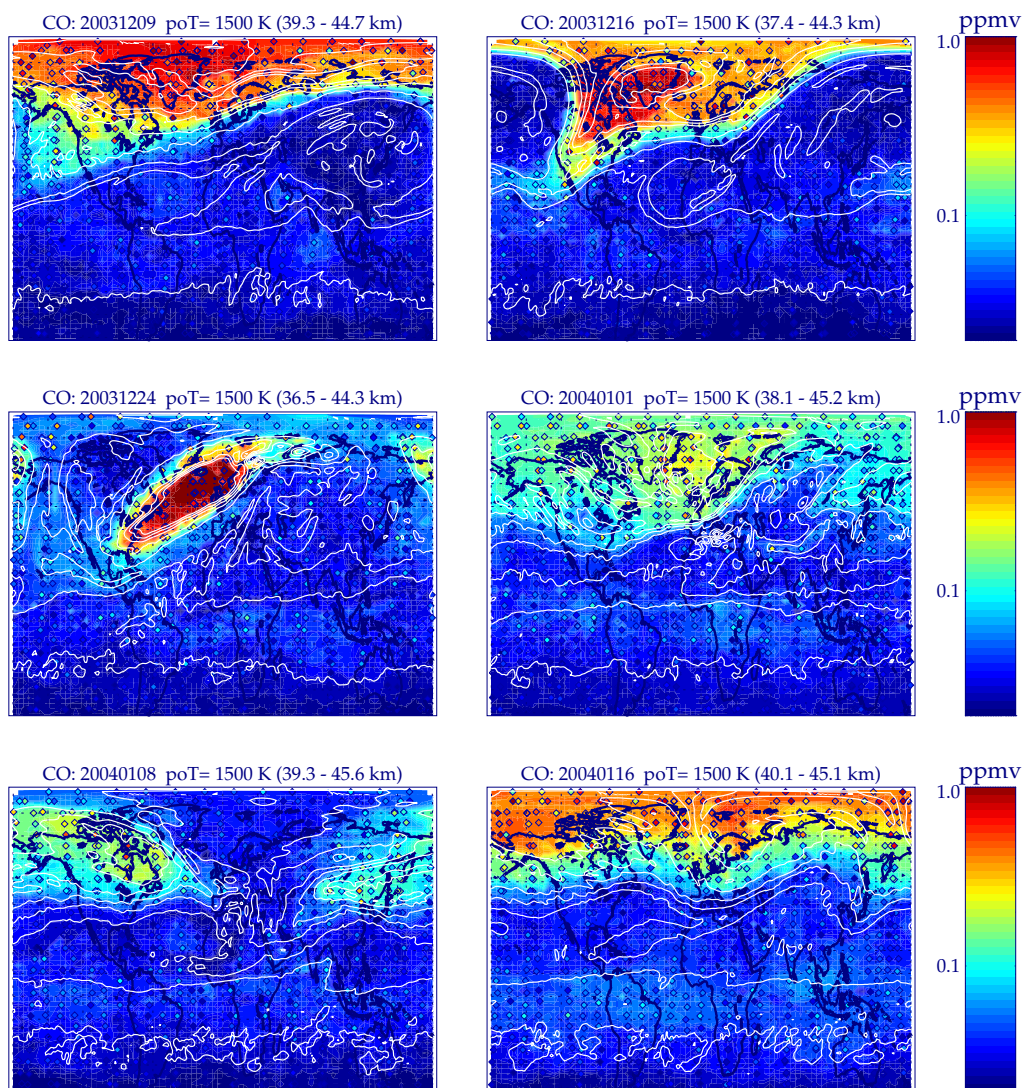
Fig. 10. As Fig. 9, but for the 1500 K isentropic surface.

around 80° N at altitudes as high as 2500 K, approximately 1000 K higher than before the warming. Mid-latitude air masses with low CO abundances were observed over the pole up to altitudes of 3500 K, particularly in the 20–40° E sector (see Fig. 11). The vortex, now located over North America's East coast, had shrunken considerably in size. While it remained very strong and conserved a high content of mesospheric air with CO vmrs around 1–2 ppmv at altitudes around 1500 K, a vortex weakening occurred in the upper stratosphere leading to a local minimum in the vortex CO abundances around 2000 K (Fig. 12, middle left panel).

With the beginning of 2004, the stratospheric vortex had nearly completely disappeared above 1500 K and mesospheric air-masses had mixed with mid-latitude air. In consequence, a rather homogeneous CO distribution with abundances of 100–200 ppbv was observed at latitudes higher than 50° N, except for the 0–90° E sector, where unmixed CO-poor mid-latitude air was dominant (see Figs. 9–12, middle right panels). Below 1500 K, however, the vortex remained well defined, though disconnected from the mesosphere, with CO abundances around 300–700 ppbv.

The influx of mid-latitude air in the 0–90° E sector led again to a very CO-poor polar region below 2000 K on 8 January (see Figs. 9–12, lower left panels). In the mesosphere, however, a moderate increase of polar CO indicate the beginning of the vortex recovery. The remnant middle stratospheric vortex was located at 50° N over the Atlantic with an elongated shape in East-West direction (see Fig. 12). During the first days of 2004, vortex air masses descended further down to approximately 1000 K, particularly in the easterly part.
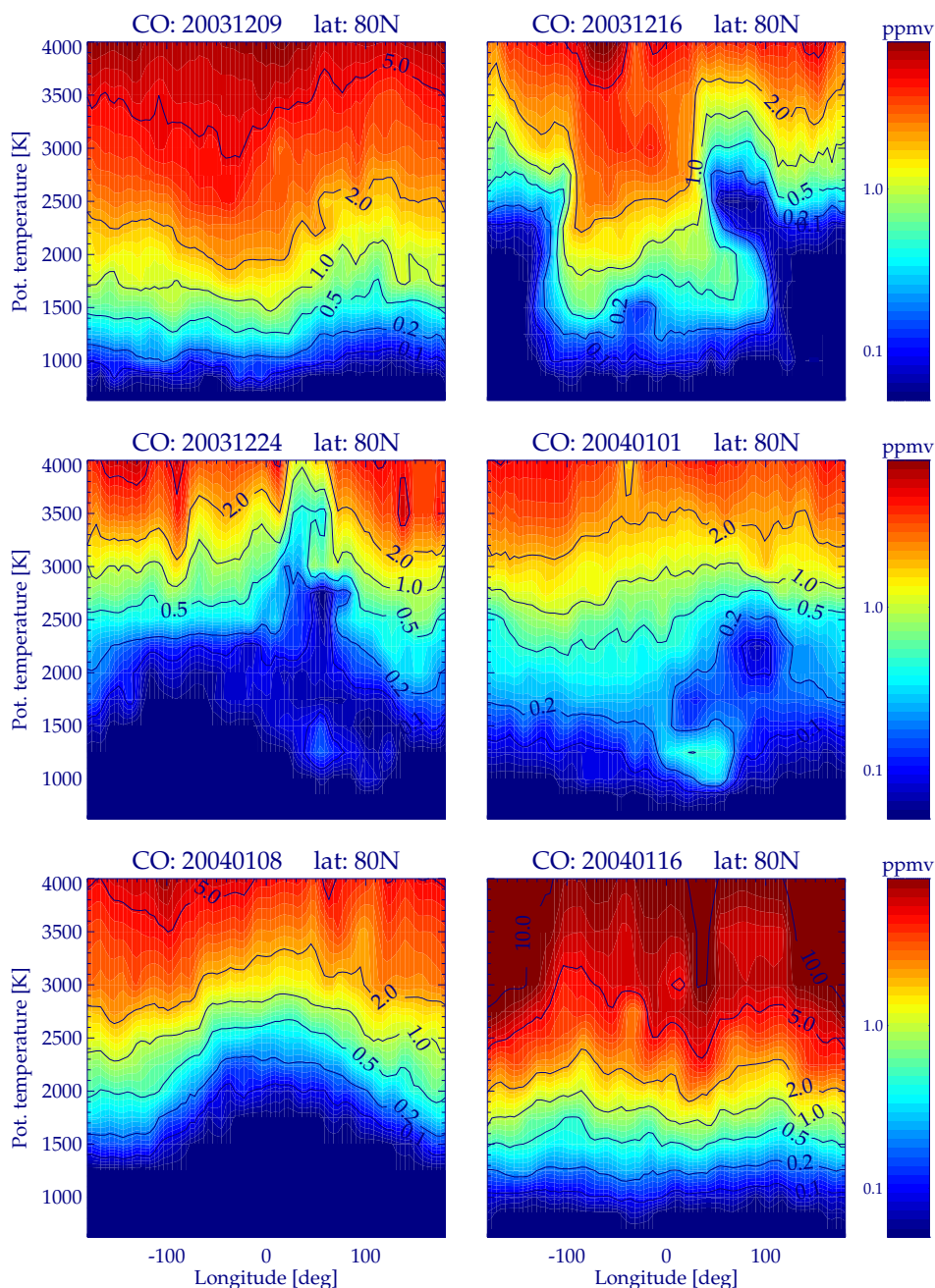
Fig. 11. Longitude–potential temperature cross section of the CO vmr at latitude 80° N constructed from MIPAS CO observations for the same days in December 2003 and January 2004 as in Fig. 10.

On 16 January, the upper stratospheric and mesospheric vortex had fully recovered and CO volume mixing ratios of up to 10 ppmv were observed at 3000 K, much larger than before the warming event (see Figs. 9–12, lower right panels). Its shape was pole-centered with a sharp vortex edge located around 70° N. At lower latitudes, a pronounced wave 2 pattern was present, particularly at altitudes below 2000 K. In consequence, the remnant middle stratospheric vortex was

weakened substantially and finally split into two parts with CO abundances not higher than 100 ppbv.

In summary, the 2003/2004 NH major warming provoked first a disruption of the upper stratospheric and mesospheric vortex, leading to a release of mesospheric air which quickly mixed up with ambient air masses, while at the same time, the middle stratospheric vortex below 1500 K was strengthened and rapid descent occurred down to altitudes around
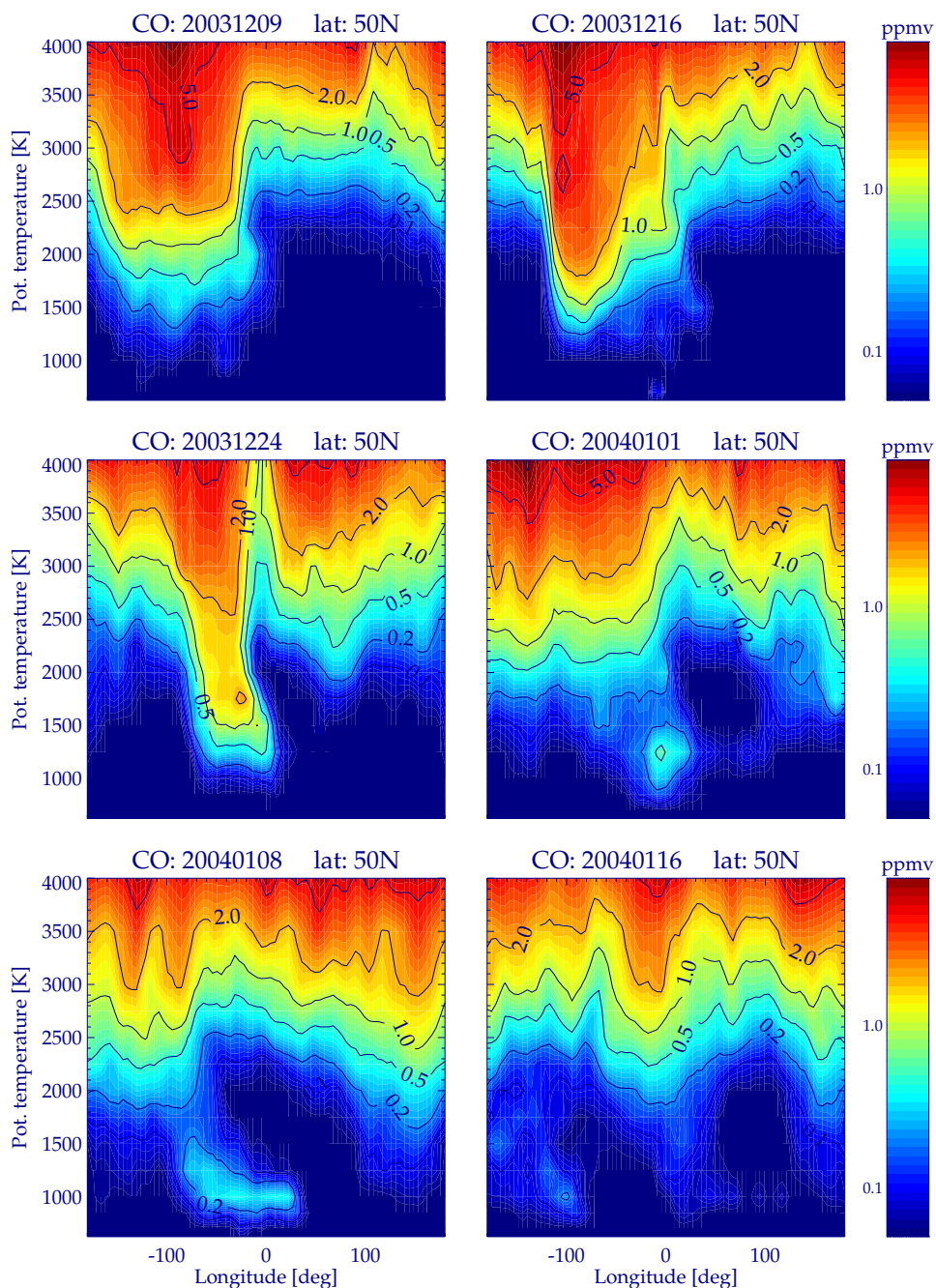
Fig. 12. As Fig. 11, but for 50° N.

1000 K. Enhanced vortex descent has also been reported for other major warming events (Manney et al., 2005b). Later in January, the vortex recovered in the USM, and mesospheric air masses filled up surprisingly fast the polar region down to 1500 K. The remnant middle stratospheric vortex, however, weakened substantially in this second step. A similar evolution of the USM vortex as in January 2004 occurred also in the 2005/2006 NH winter (Randall et al., 2006; Siskind

et al., 2007; Manney et al., 2008). In this sense, dynamical perturbations of the polar winter stratosphere, though reducing the efficiency of mesospheric tracer descent in a first instance, often provoke subsequently accelerated descent as an indirect effect which may even overcompensate the direct implications.

6   Upper tropospheric and lower stratospheric CO distributions in September–October 2003

The CO distribution in the upper troposphere is of particular interest for tracing long-range transport of polluted air masses as well as uplift processes from the boundary layer to the upper troposphere. In the lower stratosphere, global CO observations help to identify troposphere to stratosphere transport (TST) processes. CO is brought from the boundary layer to the upper troposphere by deep convection and frontal or orographic uplift. Its tropospheric lifetime of 1–2 months is short enough to differentiate polluted from clean air masses, as well as tropospheric from stratospheric air. On the other hand, its lifetime is long enough to track upper tropospheric long-range transport pathways.

Precision and horizontal sampling density of vertically resolved MIPAS CO measurements allow for a close-to-synoptic analysis of upper tropospheric CO distributions without the need of averaging over a longer time period. Here, we discuss CO distributions at pressure levels from 50–270 hPa, obtained from two 3-day observation periods during the biomass burning season in September and October 2003 (see Fig. 13). The accuracy of the smoothed CO fields shown here is in the order of 4–6 ppbv. Upper tropospheric CO abundances are quite variable, ranging from 70–90 ppbv in the background to mixing ratios higher than 140 ppbv at several "hot spots" located in the tropics and subtropics. On 9–11 September, these CO plumes were mainly located over India, Arabic peninsula, South Atlantic, Northeast Pacific, and east of Japan. On 20–22 October, highest upper tropospheric CO abundances were found over the tropical Atlantic and the Indian Ocean.

The separation from stratospheric CO abundances of generally less than 50 ppbv by a pronounced gradient coincides well with the tropopause intersection from the National Centers for Environmental Prediction (NCEP) reanalysis data (http://www.cdc.noaa.gov/cdc/data.ncep.reanalysis.html). The capability to differentiate tropospheric and stratospheric air masses is particularly well illustrated by the CO distribution at 270 hPa on 20–22 October 2003, where an outflow of subtropical tropospheric air to the Arctic was also observed (see Fig. 13, lower right panel).

In the tropical tropopause layer and lower stratosphere (100–50 hPa), we still observe enhanced CO abundances which could hint at TST. At 50 hPa, these enhancements are mainly located over Africa, Indonesia, and the Western Pacific. High CO abundances are also observed at this pressure level over the South polar region in October (see Fig. 13, upper right panel). In contrast to the tropical CO enhancements in the lowermost stratosphere, the latter are related to mesospheric air masses inside the remnant spring austral vortex which had descended down to these altitudes with the beginning of October (see also Sect. 4).

In order to interpret the inhomogeneous upper tropospheric CO distributions, with several "hot spots" in the tropics and subtropics, in the context of long-range transport pathways and uplift processes, we show in Figs. 14 and 16 the averaged CO fields obtained from the measurements for 9–11 September and 20–22 October on different pressure levels together with the corresponding wind fields from the NCEP reanalysis in the latitude range 45° S–45° N. Areas with an outgoing long-wave radiation (OLR) lower than 220 W m^{-2} are also shown as indicator for deep convection, the major uplift process for polluted air masses from the boundary layer to the upper troposphere. Additionally, we performed backward trajectory calculations with the HYbrid Single-Particle Lagrangian Integrated Trajectory (HYSPLIT) model (Draxler and Hess, 1998), based on meteorological data from the NCEP reanalysis, in order to identify potential source regions of the most pronounced CO plumes observed by MIPAS (see Figs. 15 and 17). Though the accuracy of single trajectory locations is limited to about 20% of the distance traveled (Stohl, 1998), related uncertainties are directionally unbiased for timescales larger than 5 h (Draxler, 1991) and thus are dominated by random errors, which in tendency cancel out when large ensembles are analyzed statistically. Thus, between 1000 to 2000 trajectory endpoints, located at 10 km altitude, were chosen for the representation of each of the areas where enhanced CO was observed. However, only trajectories originating at altitudes below 3.5 km were considered for further evaluation. This altitude is representative for the upper boundary of the tropical mixing layer and complies with the injection altitude for biomass burning pollutants determined by Labonne et al. (2007). Sensitivity tests have shown that the final trajectory pattern varies only marginally with the injection altitude varying between 2500 and 4500 m. The time range of 10 to 14 days proved to be sufficient to capture intercontinental transport.

Potential surface sources of the observed upper tropospheric CO plumes are related to industrial emissions and biomass burning. We thus expect the CO to be injected into the free troposphere in the vicinity of industrial or highly populated regions, as well as close to areas where biomass burning has been detected in the preceding days. The distribution of active fires as observed by the MODIS instrument on the TERRA satellite (http://firefly.geog.umd.edu/firemap/) during the period of interest indicate enhanced biomass burning activity mainly in the tropical South America, Africa, and Indonesia. The fire activity did not change significantly in the SH during September–October, while an increasing activity was detected in the tropical NH towards the end of this period.

During 9–11 September 2003 (Fig. 14), the most striking feature of the tropical upper tropospheric CO distribution was a pronounced maximum of approximately 120 ppbv which appeared consistently at pressure levels up to 100 hPa between Northwest India and the Arabic peninsula. This CO enhancement, which was enclosed by the vector wind field over this area, can be clearly attributed to the trapping of polluted air masses in the Asian monsoon anticyclone (AMA)
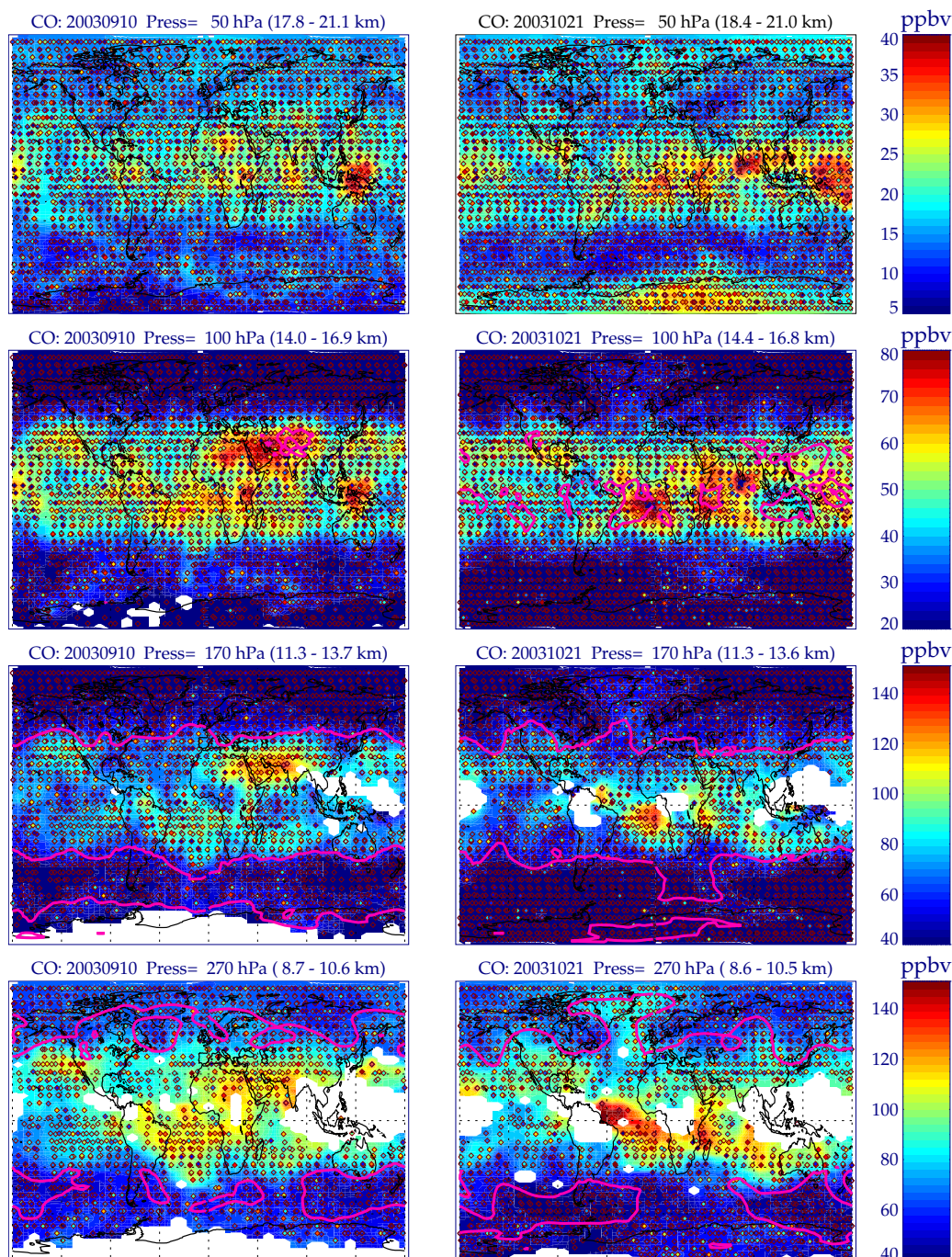
Fig. 13. Observed CO abundances at the 50, 100, 170, and 270 hPa pressure surfaces (top to bottom) on 9–11 September 2003 (left) and 20–22 October 2003 (right). Individual MIPAS observations are shown by colored diamonds. The underlaid CO fields are constructed from the observations by distance-weighted averaging of all measurements within ±10° latitude/±20° longitude around each grid point. The tropopause intersection from the NCEP reanalysis is shown by purple solid lines. White areas contain no data due to the presence of clouds.

(Li et al., 2005; Fu et al., 2006; Park et al., 2008). Our results corroborate the finding of Park et al. (2008) that this behavior extends well into the tropical tropopause level and possibly above.

At 270 hPa, strongly enhanced CO abundances were found at the easterly flank of the AMA, downwind of the extended convection zone over Southeast Asia indicated by low OLR (see Fig. 14, lower panel). Backward trajectory calculations
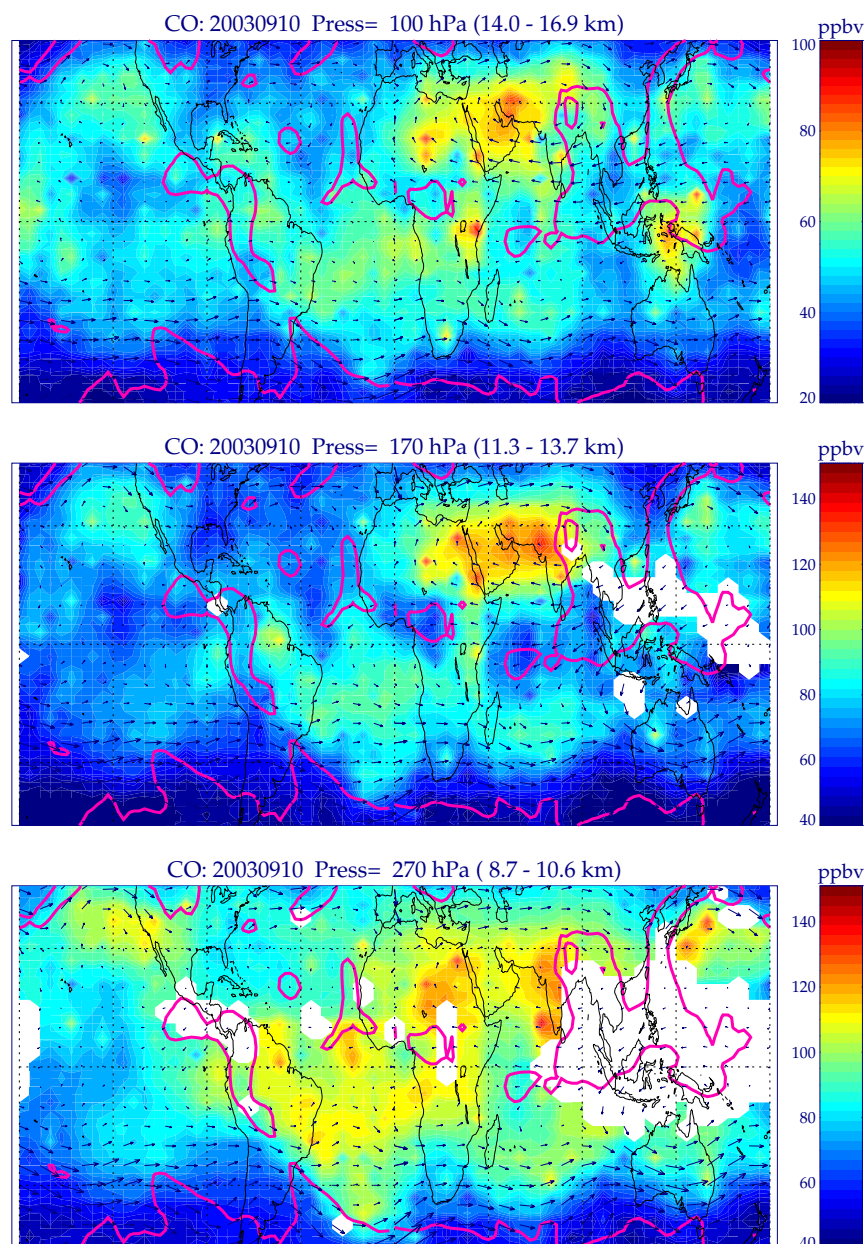
Fig. 14. Averaged CO fields constructed from observations by distance-weighted averaging of all measurements within $\pm 10°$ latitude/$\pm 20°$ longitude around each grid point at pressure levels 100, 170, and 270 hPa (top to bottom) on 9–11 September 2003 between 45° S and 45° N. Areas with OLR $<220 \, \mathrm{W \, m^{-2}}$ indicating deep convection are enclosed by purple contour lines. The vector wind fields at the corresponding pressure levels are also shown. OLR and wind field data are taken from the NCEP reanalysis.

performed for this region indicate that the polluted air was injected into the free troposphere mainly over the Bangladesh area and Southeast China (see Fig. 15, upper left panel). Since biomass burning activity was low in these regions at the beginning of September, industrial and urban emissions are the most likely source, although a smaller contribution from Indonesian biomass burning cannot be excluded. The trajectories representing polluted air parcels were lofted into the upper troposphere over the Southeast Asian convective region related to the summer monsoon.

Enhanced CO abundances were also found at 270 hPa around 10–20° N over Africa, at the westerly flank of the AMA. At a first glance, convective uplift of biomass burning emissions over the tropical West Africa (see OLR contours in Fig. 14) and subsequent northward advection appears to be the most likely source. However, the trajectory
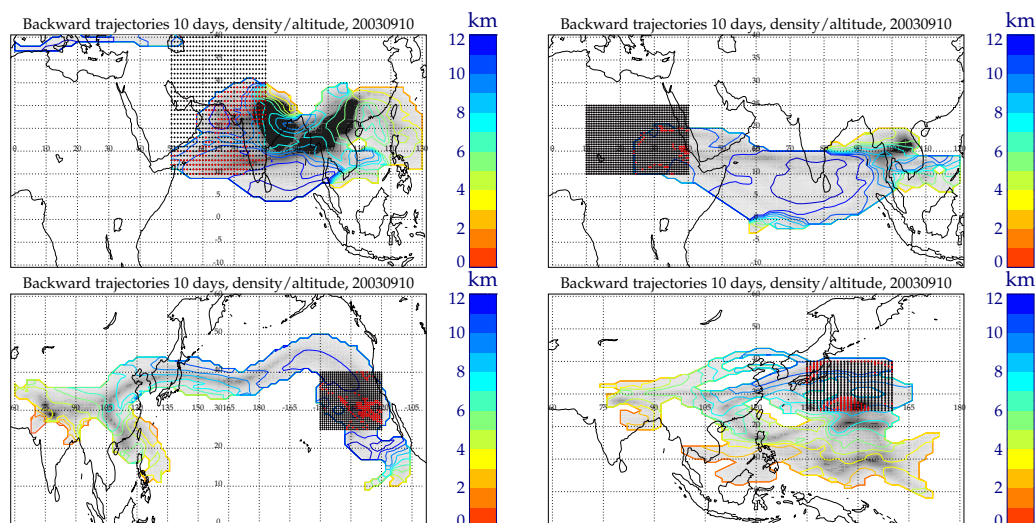
Fig. 15. Density (grey-scale shading) and mean altitude (color contour lines) of 10-day backward trajectories calculated with the HYSPLIT model, ending on 10 September 2003 at 10 km altitude over areas where CO plumes have been observed by MIPAS (indicated by dotted rectangles). For each area, about 1000 to 2000 trajectories have been calculated, but only those originating at altitudes below 3.5 km have been considered for the calculation of density and mean altitude. End points of considered and rejected trajectories, forming a dotted rectangle, are shown by red and black symbols, respectively.

calculations (Fig. 15, upper right panel) clearly show that also this CO plume originated in Southeast Asia. This is in agreement with Barret et al. (2008), who found from the assimilation of MLS CO data, taken during July 2006, into the MOCAGE chemistry transport model that the tropical easterly jet is responsible for the transport of CO-enriched air masses from India and Southeast Asia over North Africa. A smaller fraction of the trajectories, shown in the upper right panel of Fig. 15, were convectively lofted into the upper troposphere over the Southern Indian Ocean (see OLR contours in Fig. 14), far away from any pollution sources. These trajectories, ending predominantly over the Red Sea area, hint on intrusions of clean air which could explain the lower CO abundances observed at 270 hPa south of the Arabic peninsula, separating the African and the Indian plume.

Our analysis demonstrates that convective uplift of Southeast Asian pollution over the monsoon region was the major contributor to the enhanced upper tropospheric CO trapped within the AMA in September 2003. In contrast, CO abundances observed over Tibet were rather low. Thus, convective uplift driven by enhanced surface heating over the Tibetan plateau, as suggested by Fu et al. (2006), played a minor role during this period.

In the NH, upper tropospheric CO enhancements with vmrs around 120 ppbv at 270 hPa were further observed at 40° N, west of America and east of Japan. At higher altitudes, however, these plumes had considerably lower CO abundances than those observed within the AMA. Again, the corresponding backward trajectory calculations for the American plume (Fig. 15, lower left panel) indicate that

Southeast Asian pollution was the main contributor. These air masses were transported by the subtropical westerly jet across the Pacific within only a few days. In contrast to the Indian and African plume discussed above, the mean trajectory altitude increased rather slowly along the transport path, indicating that deep convection might have played a less important role. Also, the Japanese plume can be related to Southeast Asian emissions, although the trajectory calculations (Fig. 15, lower right panel) suggest a larger Indonesian contribution.

In the SH, a belt of enhanced CO was observed up to 100 hPa in the tropics and subtropics between 45° W and 90° E. These enhancements can be related to biomass burning in the equatorial South America and Africa. The plume extensions in easterly direction of their source regions showed a good correlation with the prevailing wind patterns. CO abundances inside the SH biomass burning plumes, however, were considerably lower than those found over Asia on this day.

The upper tropospheric CO distribution during 20–22 October 2003 offers a different picture (see Fig. 16). Since the AMA had completely disappeared, CO abundances over Asia were much smaller than in September. Instead, pronounced CO enhancements with vmrs higher than 150 ppbv were visible east of the biomass burning regions of South America and Central Africa. Indeed, these CO plumes had a very similar spatial distribution as C_2H_6 plumes observed by MIPAS in the same period which have been attributed to SH biomass burning (von Clarmann et al., 2007). Enhanced CO columns related to South American and African
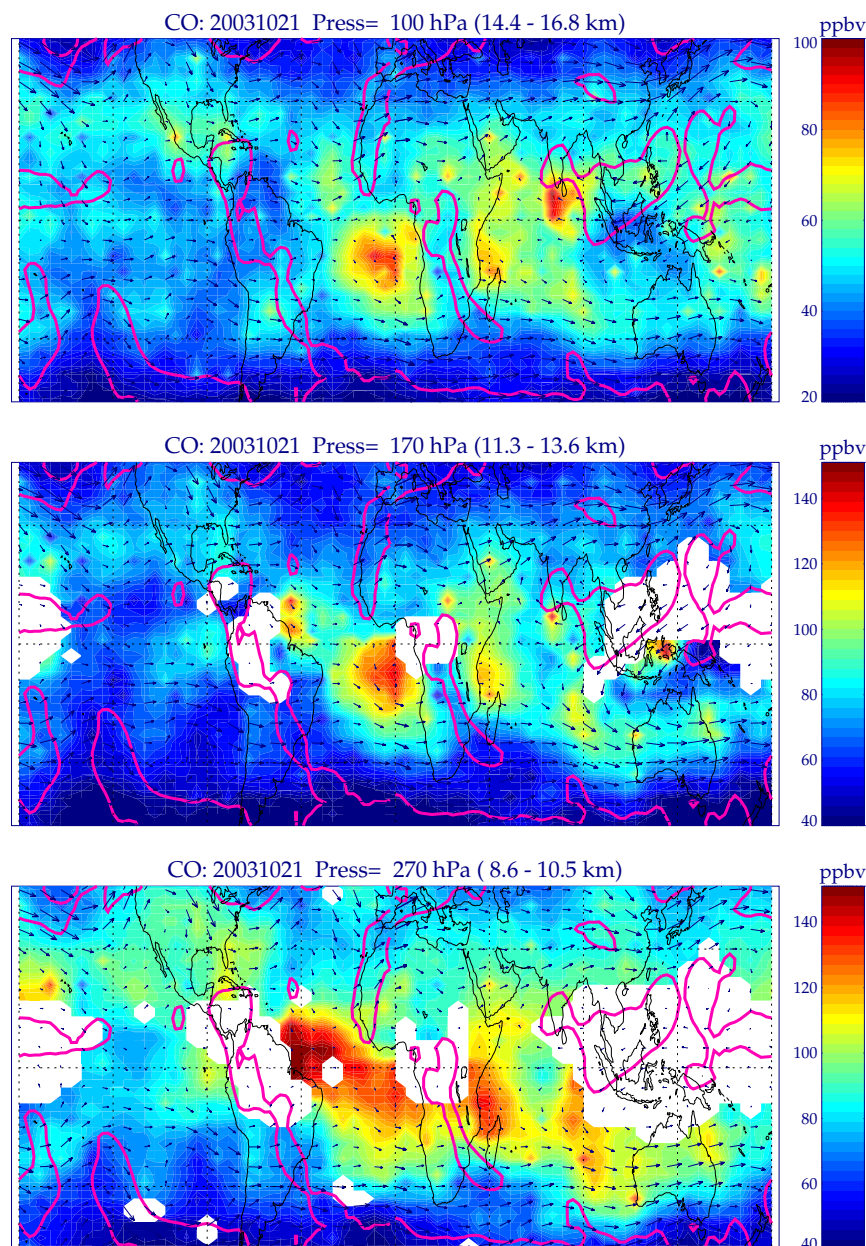
Fig. 16. As Fig. 14, but for the period of 20–22 October 2003.

biomass burning in October 2003 have also been measured by the SCIAMACHY/Envisat instrument (Gloudemans et al., 2006). The strong CO enhancements observed by MIPAS east of Northeast Brazil reached up to the 170 hPa level. The corresponding backward trajectories (Fig. 17, upper left panel) indicate that the polluted air was predominantly injected over the Amazon basin and subsequently lofted by deep convection (see also OLR contours in Fig. 16). Frontal uplift related to the tropical storm Nicholas, which was located on this day at 16° N/50° W could also have played an important role, as suggested by the high trajectory density in

its vicinity. A smaller fraction of trajectories, lofted in this region, originated in West Africa. It is thus likely, that also African biomass burning contributed to some extent to the CO plume observed east of Brazil. An important contribution of African biomass burning to CO enhancements over the equatorial Atlantic observed by ship-borne Fourier transform spectrometry in the same period has also been reported by Velazco et al. (2005).

The eastern part of the Atlantic plume, close to the African coast, reached much higher into the upper troposphere and probably even into the lower stratosphere (see Fig. 16, upper
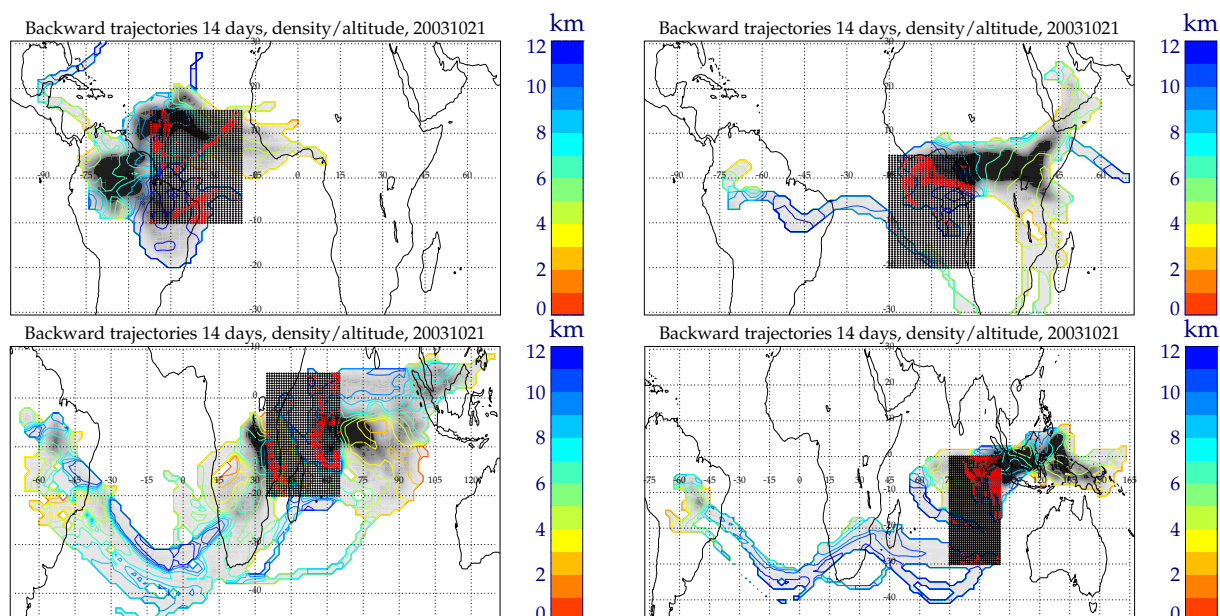
Fig. 17. Same as Fig. 15, but for 14-day backward trajectories ending on 21 October 2003 over areas where CO plumes have been observed by MIPAS.

panel). The backward trajectory calculations (Fig. 17, upper right panel) demonstrate that the major fraction of these CO enhancements had their origin in the East African biomass burning regions. Very efficient uplift by deep convection over central Africa (see OLR contours in Fig. 16) lofted the polluted air deep into the upper troposphere, where they were advected in easterly direction.

Strong CO enhancements reaching 130 ppbv were further observed east of Africa. Also this plume extended up to the tropical tropopause layer with CO abundances of 80–90 ppbv at 100 hPa. Most of the calculated backward trajectories, ending over this area, had their origin in the African biomass burning regions (see Fig. 17, lower left panel). Mean trajectory altitudes significantly below 3.5 km, indicating injections from the boundary layer, were found over Angola and Kenya. A considerable number of trajectories ending east of Africa, however, originated in South America. Similar to the transpacific transport of Asian pollution, observed in the NH during 9–11 September, fast transatlantic transport of American biomass burning pollution by the SH subtropical jet occurred in October. The trajectory calculations further indicate an important contribution of boundary layer air around 60° E. The corresponding backward trajectories originate mainly in the Eastern Indian Ocean, thus most likely representing unpolluted air masses. The MIPAS observations indeed show significantly lower CO abundances close to the equator at around 60° E, particularly at 270–170 hPa.

A CO plume with abundances around 120 ppbv at 270 hPa is also seen in Fig. 16 south of India around 90° E, extend-

ing from the equator to 30° S. The observations suggest that this plume reached up to the tropopause region, particularly in its northern part. The corresponding backward trajectory calculations (Fig. 17, lower right panel) demonstrate that the plume origin was located mainly in the Indonesian biomass burning regions. The calculations further indicate long-range transport of South American pollution which might have contributed, though to a lesser extend, to the southern part of the observed plume.

7 Conclusions

In this paper we have presented vertically resolved global CO distributions from the upper troposphere to the mesosphere which have been derived from MIPAS limb emission measurements at 4.7 μm taken during September 2003 to March 2004. These measurements, while offering the advantage of dense spatial sampling independent on illumination, are strongly affected by spatial inhomogeneities related to the high variability of CO abundances, non-LTE-effects, and spectral saturation, making the retrieval of CO mixing ratios challenging. Our retrieval approach, included in the IMK/IAA retrieval processor, addresses these issues successfully by means of several adjustments with respect to the standard algorithm which have been described in detail in Sect. 3. The derived data (version V3O_CO_9+10) provides thus accurate CO vmr distributions for any atmospheric conditions from approximately 8 to 70 km with a typical vertical resolution of 4–7 km. The estimated total retrieval error for

a single limb scan is 5–30 ppbv (15–40% for altitudes greater than 40 km and lower than 15 km and 30–90% within 15–40 km).

The temporal evolution of zonally averaged CO abundances during the observation period provides a detailed picture of the meridional circulation in the middle atmosphere, particularly of the polar winter descent. We have observed very efficient descent in the mesospheric and upper stratospheric NH polar vortex in January 2004 with vertical velocities of about 1200 km per day. This finding will help to shed some light on the ongoing discussion about the origin of the extra-ordinary NO_x enhancements observed in the same region and period (Randall et al., 2005; Rinsland et al., 2005; Hauchecorne et al., 2007; Funke et al., 2007b).

Significant amounts of mesospheric air masses persisted in the remnant spring SH polar vortex at altitudes around 25 km until the beginning of December. This is consistent with observations taken during other polar spring and summer seasons (Konopka et al., 2007; Engel et al., 2006; Stiller et al., 2008). It is thus very likely that the presence of mesospheric air masses in the lower stratosphere beyond the winter season occurs rather frequently.

The compact temporal correlation of CO and CH_4 in the tropical middle stratosphere indicates that CO abundances in this region, in contrast to polar abundances, are driven by chemistry. SAO and QBO driven oscillations of the precursor methane are expected to introduce a pronounced variability of the CO abundances, there. Upper tropospheric CO abundances show variations on an annual scale with a maximum in the Austral spring season which can be either related to seasonal trends of surface emissions or dynamical annual oscillations.

The scientific value of MIPAS CO observations for dynamical studies in the stratosphere and mesosphere, as well as in the upper troposphere and lower stratosphere (UTLS) has been further demonstrated by dedicated case studies. Quasi-synoptic stratospheric and mesospheric CO distributions observed during the NH major warming episode during December 2003 to January 2004 have provided new information on the polar vortex dynamics under perturbed conditions, particularly with respect to vertical transport processes. We have observed accelerated descent inside the middle stratospheric vortex in the first phase of the warming event, when the vortex distortion was most pronounced in the USM. In the second phase, very efficient descent took place in the recovered vortex in the USM, while the vortex disruption had propagated down to the middle stratosphere. Our findings support that dynamical perturbations of the polar winter stratosphere reduce the efficiency of mesospheric tracer descent in a first instance, but often provoke accelerated descent as an indirect effect which may even overcompensate the direct implications.

The analysis of MIPAS CO distributions in the UTLS benefit from the combination of dense spatial sampling and high accuracy, enabling the representation of global distri-

butions on a close-to-daily basis. Our case study, focussed on two 3-day periods during the SH biomass burning season in September and October 2003 confirms the general picture of UTLS dynamics obtained from previous studies with respect to transport patterns of polluted air masses and uplift mechanisms. In particular, we have observed the trapping of polluted air masses in the AMA during the Asian monsoon season which extends well up to the tropical tropopause and possibly above. We have demonstrated by means of backward trajectory calculations that the major fraction of upper tropospheric CO plumes observed by MIPAS during 9–11 September, predominantly located in the NH, was related to Southeast Asian pollution. Transpacific transport of polluted air masses was responsible for enhanced CO abundances observed over the west coast of North America. During 20–22 October, in contrast, SH biomass burning was the most important source of the major CO plumes observed over the Southern Atlantic and Indian Ocean. Polluted air masses were lofted up to the tropical tropopause layer most efficiently over Central African convective areas.

The high-lightened results obtained from approximately half a year of available V3O_CO_9+10 data open a promising perspective for future scientific studies. Data availability is currently being increasing, though progress is constrained by the high demands on computational time required by the inversion of IR limb emission measurements under non-LTE conditions. Despite of this restriction, the coverage of the "high resolution" period 2002–2004, as well as the extension to "reduced resolution" measurement obtained since 2005 is envisaged in the near future, being particularly important for the analysis of the inter-annual dynamical variability in the lower and middle atmosphere.

References

Barret, B., Ricaud, P., Mari, C., Attié, J.-L., Bousserez, N., Josse, B., Flochmoën, E. L., Livesey, N. J., Massart, S., Peuch, V.-H., Piacentini, A., Sauvage, B., Thouret, V., and Cammas, J.-P.: Transport pathways of CO in the African upper troposphere during the monsoon season: a study based upon the assimilation

of spaceborne observations, Atmos. Chem. Phys., 8, 3231–3246, 2008, http://www.atmos-chem-phys.net/8/3231/2008/.

Brasseur, G. and Solomon, S.: Aeronomy of the Middle Atmosphere, Atmospheric Science Library, D. Reidel Publishing Company, Dordrecht, Holland, second edn., 452 pp., 1986.

Buchwitz, M., Rozanov, V. V., and Burrows, J.: A near infrared optimized DOAS method for the fast global retrieval of atmospheric CH_4, CO, CO_2, H_2O, and N_2O total column amounts from SCIAMACHY/ENVISAT-1 nadir radiances, J. Geophys. Res., 105, 15231–15246, 2000.

Clerbaux, C., Coheur, P.-F., Hurtmans, D., Barret, B., Carleer, M., Semeniuk, R. C. K., McConnell, J. C., Boone, C., and Bernath, P.: Carbon monoxide distribution from the ACE-FTS solar occultation measurements, Geophys. Res. Lett., 32, L16S01, doi: 10.1029/2005GL022394, 2005.

Clerbaux, C., George, M., Turquety, S., Walker, K. A., Barret, B., Bernath, P., Boone, C., Borsdorff, T., Cammas, J. P., Catoire, V., Coffey, M., Coheur, P.-F., Deeter, M., Mazière, M. D., Drummond, J., Duchatelet, P., Dupuy, E., de Zafra, R., Eddounia, F., Edwards, D. P., Emmons, L., Funke, B., Gille, J., Griffith, D. W. T., Hannigan, J., Hase, F., Höpfner, M., Jones, N., Kagawa, A., Kasai, Y., Kramer, I., Flochmoën, E. L., Livesey, N. J., López-Puertas, M., Luo, M., Mahieu, E., Murtagh, D., Nédélec, P., Pazmino, A., Pumphrey, H., Rinsland, P. R. C. P., Robert, C., Schneider, M., Senten, C., Stiller, G., Strandberg, A., Strong, K., Sussmann, R., Thouret, V., Urban, J., and Wiacek, A.: CO measurements from the ACE-FTS satellite instrument: data analysis and validation using ground-based, airborne and spaceborne observations, Atmos. Chem. Phys., 8, 2569–2594, 2008, http://www.atmos-chem-phys.net/8/2569/2008/.

Draxler, R. R.: The accuracy of trajectories during ANATEX calculated using dynamic model analyses versus rawinsonde observations, J. Appl. Meteorol., 30, 1446–1467, 1991.

Draxler, R. R. and Hess, G. D.: An overview of the HYSPLIT 4 modelling system for trajectories, dispersion and deposition, Aust. Meteorol. Mag., 47, 295–3008, 1998.

Dupuy, E., Urban, J., Ricaud, P., Flochmoën, E. L., Lautié, N., Murtagh, D., de la Nöe, J., Amraoui, L. E., Eriksson, P., Forkman, P., Frisk, U., Jégou, F., Jiménez, C., and Olberg, M.: Strato-mesospheric measurements of carbon monoxide with the Odin sub-millimetre radiometer: Retrieval and first results, Geophys. Res. Lett., 31, L20101, doi:10.1029/2004GL020558, 2004.

Echle, G., von Clarmann, T., Dudhia, A., Flaud, J.-M., Funke, B., Glatthor, N., Kerridge, B., López-Puertas, M., Martín-Torres, F. J., and Stiller, G. P.: Optimized spectral microwindows for data analysis of the Michelson Interferometer for Passive Atmospheric Sounding on the Environmental Satellite, Appl. Optics, 39, 5531–5540, 2000.

Edwards, D. P., Emmons, L. K., Hauglustaine, D. A., Chu, D. A., Gille, J. C., Kaufman, Y. J., Pétron, G., Yurganov, L. N., Giglio, L., Deeter, M. N., Yudin, V., Ziskin, D. C., Warner, J., Lamarque, J.-F., Francis, G. L., Ho, S. P., Mao, D., Chen, J., Grechko, E. I., and Drummond, J. R.: Observations of carbon monoxide and aerosols from the Terra satellite: Northern Hemisphere variability, J. Geophys. Res., 109, D24202, doi:10.1029/2004JD004727, 2004.

Engel, A., Möbius, T., Haase, H.-P., Bönisch, H., Wetter, T., Schmidt, U., Levin, I., Reddmann, T., Oelhaf, H., Wetzel, G., Grunow, K., Huret, N., and Pirre, M.: Observation of meso-

spheric air inside the arctic stratospheric polar vortex in early 2003, Atmos. Chem. Phys., 6, 267–282, 2006, http://www.atmos-chem-phys.net/6/267/2006/.

European Space Agency: Envisat, MIPAS An instrument for atmospheric chemistry and climate research, ESA Publications Division, ESTEC, P.O. Box 299, 2200 AG Noordwijk, The Netherlands, SP-1229, 2000.

Filipiak, M. J., Harwood, R. S., Jiang, J. H., Li, Q., Livesey, N. J., Manney, G. L., Read, W. G., Schwartz, M. J., Waters, J. W., and Wu, D. L.: Carbon monoxide measured by the EOS Microwave Limb Sounder on Aura: First results, Geophys. Res. Lett., 32, L14825, doi:10.1029/2005GL022765, 2005.

Fischer, H., Birk, M., Blom, C., Carli, B., Carlotti, M., von Clarmann, T., Delbouille, L., Dudhia, A., Ehhalt, D., Endemann, M., Flaud, J. M., Gessner, R., Kleinert, A., Koopmann, R., Langen, J., López-Puertas, M., Mosner, P., Nett, H., Oelhaf, H., Perron, G., Remedios, J., Ridolfi, M., Stiller, G., and Zander, R.: MIPAS: an instrument for atmospheric and climate research, Atmos. Chem. Phys., 8, 2151–2188, 2008, http://www.atmos-chem-phys.net/8/2151/2008/.

Frankenberg, C., Platt, U., and Wagner, T.: Retrieval of CO from SCIAMACHY onboard ENVISAT: detection of strongly polluted areas and seasonal patterns in global CO abundances, Atmos. Chem. Phys., 5, 1639–1644, 2005, http://www.atmos-chem-phys.net/5/1639/2005/.

Fu, R., Hu, Y., Wright, J. S., Jiang, J. H., Dickinson, R. E., Chen, M., Filipiak, M., Read, W. G., Waters, J. W., and Wu, D. L.: Short circuit of water vapor and polluted air to the global stratosphere by convective transport over the Tibetan Plateau, Proc. Natl. Acad. Sci. USA, 103, 5664–5669, doi:10.1073/pnas.0601584103, 2006.

Funke, B., López-Puertas, M., Stiller, G. P., von Clarmann, T., and Höpfner, M.: A new non–LTE Retrieval Method for Atmospheric Parameters From MIPAS–ENVISAT Emission Spectra, Adv. Space Res., 27, 1099–1104, 2001.

Funke, B., Martín-Torres, F. J., López-Puertas, M., Höpfner, M., Hase, F., López-Valverde, M. Á., and García-Comas, M.: A generic non–LTE population model for MIPAS–ENVISAT data analysis, vol. 4, abstracts of the Contributions of the European Geophysical Society, Nice, France, 21–26 April 2002, CD-ROM, ISSN:1029–7006, 2002.

Funke, B., López-Puertas, M., Gil-López, S., von Clarmann, T., Stiller, G. P., Fischer, H., and Kellmann, S.: Downward transport of upper atmospheric NO_X into the polar stratosphere and lower mesosphere during the Antarctic 2003 and Arctic 2002/2003 winters, J. Geophys. Res., 110, D24308, doi:10.1029/2005JD006463, 2005.

Funke, B., López-Puertas, M., , Bermejo-Pantaleón, D., von Clarmann, T., Stiller, G. P., Höpfner, M., Grabowski, U., and Kaufmann, M.: Analysis of nonlocal thermodynamic equilibrium CO 4.7 μm fundamental, isotopic and hot band emissions measured by the Michelson Interferometer for Passive Atmospheric Sounding on Envisat, J. Geophys. Res., 112, D11305, doi:10.1029/2006JD007933, 2007a.

Funke, B., López-Puertas, M., Fischer, H., Stiller, G. P., von Clarmann, T., Wetzel, G., Carli, B., and Belotti, C.: Comment on 'Origin of the January–April 2004 increase in stratospheric NO_2 observed in northern polar latitudes' by J.-B. Renard et al., Geophys. Res. Lett., 34, L07813, doi:10.1029/2006GL027518,

2007b.

Garcia, R. R.: A Numerical Model of the Zonally Averaged Dynamical and Chemical Structure of the middle Atmosphere, J. Geophys. Res., 88, 1379–1400, 1983.

Garcia, R. R., Marsh, D. R., Kinnison, D. E., Boville, B. A., and Sassi, F.: Simulation of secular trends in the middle atmosphere, J. Geophys. Res., 112, D09301, doi:10.1029/2006JD007485, 2007.

Glatthor, N., von Clarmann, T., Fischer, H., Funke, B., Grabowski, U., Höpfner, M., Kellmann, S., Kiefer, M., Linden, A., Milz, M., Steck, T., Stiller, G. P., Mengistu Tsidu, G., and Wang, D. Y.: Mixing processes during the Antarctic vortex split in September/October 2002 as inferred from source gas and ozone distributions from ENVISAT-MIPAS, J. Atmos. Sci., 62, 787–800, 2005.

Gloudemans, A. M. S., Krol, M. C., Meirink, J. F., de Laat, A. T. J., van der Werf, G. R., Schrijver, H., van den Broek, M. M. P., and Aben, I.: Evidence for long-range transport of carbon monoxide in the Southern Hemisphere from SCIAMACHY observations, Geophys. Res. Lett., 33, L16807, doi:10.1029/2006GL026804, 2006.

Gloudemans, A. M. S., Schrijver, H., Hasekamp, O. P., and Aben, I.: Error analysis for CO and CH_4 total column retrievals from SCIAMACHY $2.3\,\mu m$ spectra, Atmos. Chem. Phys., 8, 3999–4017, 2008, http://www.atmos-chem-phys.net/8/3999/2008/.

Gunson, M. R., Farmer, C. B., Norton, R. H., Zander, R., Rinsland, C. P., Shaw, J. H., and Gao, B. C.: Measurements of CH_4, N_2O, CO, H_2O, and O_3 in the middle atmosphere by the Atmospheric Trace Molecule Spectroscopy experiment on Spacelab 3, J. Geophys. Res., 95, 13867–13882, 1990.

Hauchecorne, A., Bertaux, J.-L., Dalaudier, F., Russell III, J. M., Mlynczak, M. G., Kyrölä, E., and Fussen, D.: Large increase of NO_2 in the north polar mesosphere in January-February 2004: Evidence of a dynamical origin from GOMOS/ENVISAT and SABER/TIMED data, Geophys. Res. Lett., 34, L03810, doi:10.1029/2006GL027628, 2007.

Jin, J. J., Semeniuk, K., Beagley, S. R., Fomichev, V. I., Jonsson, A. I., McConnell, J. C., Urban, J., Murtagh, D., Manney, G. L., Boone, C. D., Bernath, P. F., Walker, K. A., Barret, B., Ricaud, P., and Dupuy, E.: Comparison of CMAM simulations of carbon monoxide (CO), nitrous oxide (N_2O), and methane (CH_4) with observations from Odin/SMR, ACE-FTS, and Aura/MLS, Atmos. Chem. Phys. Discuss., 8, 13063–13123, 2008, http://www.atmos-chem-phys-discuss.net/8/13063/2008/.

Kaufmann, M., Gil-López, S., López-Puertas, M., Funke, B., García-Comas, M., Glatthor, N., Grabowski, U., Höpfner, M., Stiller, G. P., von Clarmann, T., Koukouli, M. E., Hoffmann, L., and Riese, M.: Vibrationally excited ozone in the middle atmosphere, J. Atmos. Solar-Terr. Phys., 68, 202–212, doi:10.1016/j.jastp.2005.10.006, 2006.

Konopka, P., Engel, A., Funke, B., Müller, R., Grooß, J.-U., Günther, G., Wetter, T., Stiller, G. P., von Clarmann, T., Glatthor, N., Oelhaf, H., Wetzel, G., López-Puertas, M., Pirre, M., Huret, N., and Riese, M.: Ozone loss driven by nitrogen oxides and triggered by stratospheric warmings can outweigh the effect of halogens, J. Geophys. Res., 112, D05105, doi:10.1029/2006JD007064, 2007.

Labonne, M., Bréon, F., and Chevallier, F.: Injection height of biomass burning aerosols as seen from a spaceborne lidar, Geo-

phys. Res. Lett., 34, L11806, doi:10.1029/2007GL029311, 2007.

Li, Q., Jiang, J. H., Wu, D. L., Read, W. G., Livesey, N. J., Waters, J. W., Zhang, Y., Wang, B., Filipiak, M. J., Davis, C. P., Turquety, S., Wu, S., Park, R. J., Yantosca, R. M., and Jacob, D. J.: Convective outflow of South Asian pollution: A global CTM simulation compared with EOS MLS observations, Geophys. Res. Lett., 32, L14826, doi:10.1029/2005GL022762, 2005.

López-Puertas, M. and Taylor, F. W.: Non-LTE radiative transfer in the Atmosphere, World Scientific Pub., Singapore, 487 pp., 2001.

López-Puertas, M., Funke, B., Gil-López, S., López-Valverde, M. A., von Clarmann, T., Fischer, H., Oelhaf, H., Stiller, G. P., Kaufmann, M., Koukouli, M. E., and Flaud, J.-M.: Atmospheric non-local thermodynamic equilibrium emissions as observed by the Michelson Interferometer for Passive Atmospheric Sounding (MIPAS), C. R. Phys., 6, 848–863, doi:10.1016/j.crhy.2005.07.012, 2005.

López-Valverde, M. Á., López-Puertas, M., Remedios, J. J., Rodgers, C. D., Taylor, F. W., Zipf, E. C., and Erdman, P. W.: Validation of measurements of carbon monoxide from the Improved Stratospheric and Mesospheric Sounder, J. Geophys. Res., 101, 9929–9955, 1996.

Manney, G. L., Krüger, K., Sabutis, J. L., Sena, S. A., and Pawson, S.: The remarkable 2003–2004 winter and other recent warm winters in the Arctic stratosphere since the late 1990s, J. Geophys. Res., 110, D04107, doi:10.1029/2004JD005367, 2005a.

Manney, G. L., Sabutis, J. L., Allen, D. R., Lahoz, W. A., Scaife, A. A., Randall, C. E., Pawson, S., Naujokat, B., and Swinbank, R.: Simulations of dynamics and transport during the September 2002 Antarctic major warming, J. Atmos. Sci., 62, 690–707, 2005b.

Manney, G. L., Krueger, K., Minschwaner, S. P. K., Schwartz, M. J., Daffer, W., Livesey, N. J., Mlynczak, M. G., Remsberg, E., Russell, J. M., and Waters, J. W.: The evolution of the stratopause during the 2006 major warming: satellite data and assimilated meteorological analyses, J. Geophys. Res., 113, D11115, doi:10.1029/2007JD009097, 2008.

Nassar, R., Bernath, P. F., Boone, C. D., Manney, G. L., McLeod, S. D., Rinsland, C. P., Skelton, R., and Walker, K. A.: Stratospheric abundances of water and methane based on ACE–FTS measurements, Geophys. Res. Lett., 32, L15S04, doi:10.1029/2005GL022383, 2005.

Nett, H., Carli, B., Carlotti, M., Dudhia, A., Fischer, H., Flaud, J.-M., Perron, G., Raspollini, P., and Ridolfi, M.: MIPAS Ground Processor and Data Products, in: Proc. IEEE 1999 International Geoscience and Remote Sensing Symposium, 28 June – 2 July 1999, Hamburg, Germany, 1692–1696, 1999.

Park, M., Randel, W. J., Emmons, L. K., Bernath, P. F., Walker, K. A., and Boone, C. D.: Chemical isolation in the Asian monsoon anticyclone observed in Atmospheric Chemistry Experiment (ACE-FTS) data, Atmos. Chem. Phys., 8, 757–764, 2008, http://www.atmos-chem-phys.net/8/757/2008/.

Randall, C. E., Harvey, V. L., Manney, G. L., Orsolini, Y. J., Codrescu, M., Sioris, C., Brohede, S., Haley, C. S., Gordley, L. L., Zawodny, J. M., and Russell III, J. M.: Stratospheric effects of energetic particle precipitation in 2003–2004, Geophys. Res. Lett., 32, L05802, doi:10.1029/2004GL022003, 2005.

Randall, C. E., Harvey, V. L., Singleton, C. S., Bernath, P. F., Boone, C. D., and Kozyra, J. U.: Enhanced NO_x in 2006 linked to

strong upper stratospheric Arctic vortex, Geophys. Res. Lett., 22, L18811, doi:10.1029/2006GL027160, 2006.

Rinsland, C. P., Boone, C., Nassar, R., Walker, K., Bernath, P., McConnell, J. C., and Chiou, L.: Atmospheric Chemistry Experiment (ACE) Arctic stratospheric measurements of NO_x during February and March 2004: Impact of intense solar flares, Geophys. Res. Lett., 32, L16S05, doi:10.1029/2005GL022425, 2005.

Rinsland, C. P., Luo, M., Logan, J. A., Beer, R., Worden, H., Kulawik, S. S., Rider, D., Osterman, G., Gunson, M., Eldering, A., Goldman, A., Shepherd, M., Clough, S. A., Rodgers, C., Lampel, M., and Chiou, L.: Nadir measurements of carbon monoxide distributions by the Tropospheric Emission Spectrometer instrument onboard the Aura Spacecraft: Overview of analysis approach and examples of initial results, Geophys. Res. Lett., 33, L22806, doi:10.1029/2006GL027000, 2006.

Rodgers, C. D.: Inverse Methods for Atmospheric Sounding: Theory and Practice, vol. 2, Series on Atmospheric, Oceanic and Planetary Physics, F. W. Taylor, ed., World Scientific, 2000.

Rosenfield, J. E., Newman, P. A., and Schoeberl, M. R.: Computations of diabatic descent in the stratospheric polar vortex, J. Geophys. Res., 99, 16677–16689, 1994.

Schoeberl, M. R., Duncan, B. N., Douglass, A. R., Waters, J., Livesey, N., Read, W., and Filipiak, M.: The carbon monoxide tape recorder, Geophys. Res. Lett., 33, L12811, doi:10.1029/2006GL026178, 2006.

Siskind, D. E.: Atmospheric science across the Stratopause, vol. 123, Geophysical Monograph, chap. On the coupling between middle and upper atmospheric odd nitrogen, 101–116, American Geophysical Union, 2000.

Siskind, D. E., Eckermann, S. D., Coy, L., McCormack, J. P., and Randall, C. E.: On recent inter-annual variability of the Arctic winter mesosphere: Implications for tracer descent, Geophys. Res. Lett., 34, L09806, doi:10.1029/2007GL029293, 2007.

Spang, R., Remedios, J. J., and Barkley, M. P.: Colour indices for the detection and differentiation of cloud types in infra–red limb emission spectra, Adv. Space Res., 3, 1041–1047, doi:10.1016/S0273-1177(03)00585-4, 2004.

Steck, T.: Methods for determining regularization for atmospheric retrieval problems, Appl. Optics, 41, 1788–1797, 2002.

Stiller, G. P., von Clarmann, T., Funke, B., Glatthor, N., Hase, F., Höpfner, M., and Linden, A.: Sensitivity of trace gas abundances retrievals from infrared limb emission spectra to simplifying approximations in radiative transfer modelling, J. Quant. Spectrosc. Ra., 72, 249–280, 2002.

Stiller, G. P., v. Clarmann, T., Höpfner, M., Glatthor, N., Grabowski, U., Kellmann, S., Kleinert, A., Linden, A., Milz, M., Reddmann, T., Steck, T., Fischer, H., Funke, B., López-Puertas, M., and Engel, A.: Global distribution of mean age of stratospheric air from MIPAS SF_6 measurements, Atmos. Chem. Phys., 8, 677–695, 2008, http://www.atmos-chem-phys.net/8/677/2008/.

Stohl, A.: Computation, accuracy and application of trajectories – A review and bibliography, Atmos. Environ., 32, 947–996, 1998.

Tikhonov, A.: On the solution of incorrectly stated problems and method of regularization, Dokl. Akad. Nauk. SSSR, 151, 501–504, 1963.

Turquety, S., Hadji-Lazaro, J., Clerbaux, C., Hauglustaine, D. A., Clough, S. A., Cassé, V., Schlüssel, P., and Mégie, G.: Operational trace gas retrieval algorithm for the Infrared Atmospheric Sounding Interferometer, J. Geophys. Res., 109, D21301, doi:10.1029/2004JD004821, 2004.

Velazco, V., Notholt, J., Warneke, T., Lawrence, M., Bremer, H., Drummond, J., Schulz, A., Krieg, J., and Schrems, O.: Latitude and altitude variability of carbon monoxide in the Atlantic detected from ship-borne Fourier transform spectrometry, model, and satellite data, J. Geophys. Res., 110, D09306, doi:10.1029/2004JD005351, 2005.

von Clarmann, T., Ceccherini, S., Doicu, A., Dudhia, A., Funke, B., Grabowski, U., Hilgers, S., Jay, V., Linden, A., López-Puertas, M., Martín-Torres, F.-J., Payne, V., Reburn, J., Ridolfi, M., Schreier, F., Schwarz, G., Siddans, R., and Steck, T.: A blind test retrieval experiment for infrared limb emission spectrometry, J. Geophys. Res., 108, 4746, doi:10.1029/2003JD003835, 2003a.

von Clarmann, T., Glatthor, N., Grabowski, U., Höpfner, M., Kellmann, S., Kiefer, M., Linden, A., Mengistu Tsidu, G., Milz, M., Steck, T., Stiller, G. P., Wang, D. Y., Fischer, H., Funke, B., Gil-López, S., and López-Puertas, M.: Retrieval of temperature and tangent altitude pointing from limb emission spectra recorded from space by the Michelson Interferometer for Passive Atmospheric Sounding (MIPAS), J. Geophys. Res., 108, 4736, doi:10.1029/2003JD003602, 2003b.

von Clarmann, T., Glatthor, N., Koukouli, M. E., Stiller, G. P., Funke, B., Grabowski, U., Höpfner, M., Kellmann, S., Linden, A., Milz, M., Steck, T., and Fischer, H.: MIPAS measurements of upper tropospheric C_2H_6 and O_3 during the southern hemispheric biomass burning season in 2003, Atmos. Chem. Phys., 7, 5861–5872, 2007, http://www.atmos-chem-phys.net/7/5861/2007/.